SPECIAL
RELAMPAGO-CACTI
COLLECTION

Influences of the South American Low-Level Jet on the Convective Environment in Central Argentina Using a Convection-Permitting Simulation

CLAYTON R. S. SASAKI,[a] ANGELA K. ROWE,[b] LYNN A. MCMURDIE,[a] ADAM C. VARBLE,[c] AND ZHIXIAO ZHANG[d,e]

[a] *Department of Atmospheric Sciences, University of Washington, Seattle, Washington*
[b] *Department of Atmospheric and Oceanic Sciences, University of Wisconsin–Madison, Madison, Wisconsin*
[c] *Atmospheric Sciences and Global Change Division, Pacific Northwest National Laboratory, Richland, Washington*
[d] *Department of Atmospheric Sciences, University of Utah, Salt Lake City, Utah*
[e] *Atmospheric, Oceanic and Planetary Physics, University of Oxford, Oxford, United Kingdom*

(Manuscript received 13 June 2023, in final form 27 December 2023, accepted 29 December 2023)

ABSTRACT: This study documents the spatial and temporal distribution of the South American low-level jet (SALLJ) and quantifies its impact on the convective environment using a 6.5-month convection-permitting simulation during the Remote Sensing of Electrification, Lightning, And Mesoscale/Microscale Processes with Adaptive Ground Observations and Clouds, Aerosols, and Complex Terrain Interactions (RELAMPAGO-CACTI) campaigns. Overall, the simulation reproduces the observed SALLJ characteristics in central Argentina near the Sierras de Córdoba (SDC), a focal point for terrain-focused upscale growth. SALLJs most frequently occur in the summer with maxima to the northwest and east of the SDC and minima over the higher terrain. The shallower SALLJs (<1750 m) have a strong overnight skew, while the elevated jets are more equally spread throughout the day. SALLJ periods often have higher amounts of low-level moisture and instability compared to non-SALLJ periods, with these impacts increasing over time when the SALLJ is present and decreasing afterward. The SALLJ may enhance low-level wind shear magnitudes (particularly when accounting for the jet height); however, enhancement is somewhat limited due to the presence of speed shear in most situations. SALLJ periods are associated with low-level directional shear favorable for organized convection and an orientation of cloud-layer wind shear parallel to the terrain, which could favor upscale growth. A case study is shown in which the SALLJ influenced both the magnitude and direction of wind shear concurrent with convective upscale growth near the SDC. This study highlights the complex relationship between the SALLJ and its impacts during periods of widespread convection.

SIGNIFICANCE STATEMENT: Areas of enhanced low-level winds, or low-level jets, likely promote favorable conditions for upscale growth, the processes by which storms grow larger. Central Argentina is an ideal place to study the influence of low-level jets on upscale growth as storms often stay connected to the Sierras de Córdoba Mountain range, growing over a relatively small area. This study uses model data to describe the distribution and impact of the South American low-level jet on the storm environment. The South American low-level jet is frequently found near the Sierras de Córdoba, and moisture and convective instability increase when it is present. However, the jet's impact on other conditions important for upscale growth, such as vertical wind shear, is not as straightforward.

KEYWORDS: South America; Convective storms/systems; Wind shear; Mesoscale processes; Mesoscale models; Model evaluation/performance

1. Introduction

From satellite observations it is estimated that mesoscale convective systems (MCSs) are responsible for over half of all annual precipitation in the tropics and subtropics (Nesbitt et al. 2006; Schumacher and Rasmussen 2020) and 30%–70% of warm season precipitation in the United States (Fritsch et al. 1986). Despite their importance to weather and climate, forecasting of MCSs has been shown to have low skill (e.g., Weisman et al. 2013; Peters et al. 2017). Accurate representation of convective upscale growth, the processes by which discrete deep convection transitions into large MCSs, is essential for improving prediction of MCSs (e.g., Coniglio et al. 2010).

Studies, mainly focused on the United States, have put forward hypotheses for environments which support convective upscale growth. Generally, synoptic-scale lifting from upper-level troughs promotes cloud organization (Tao and Simpson 1984), and synoptic-scale convergence, often from frontal zones,

Denotes content that is immediately available upon publication as open access.

Corresponding author: Clayton R. S. Sasaki, crs326@uw.edu

DOI: 10.1175/MWR-D-23-0122.1

prolongs MCS lifetimes (Crook and Moncrieff 1988). Additionally, high amounts of moisture and strong instability are necessary for the deep, long-lived convection associated with MCSs. Low-level jets (LLJs) can provide these favorable conditions, transporting low-level moisture and heat, increasing instability, and leading to mesoscale convergence at the terminus of the jet (Gebauer et al. 2018; Stelten and Gallus 2017; Tuttle and Davis 2006; Houze 2004; Higgins et al. 1997; Wu and Raman 1998; Stensrud 1996).

Vertical wind shear also plays an important role in the upscale growth of convection. The orientation of cloud-layer winds and vertical wind shear relative to the convection is likely important for determining if convection grows upscale and the rate of organization. For storms that initiate along a boundary, deep-layer shear parallel to the initiating boundary leads to longer residence times within the zone of forcing and also aligns cold pools to promote organization and growth (Cohen et al. 2007; Dial et al. 2010). Wind shear at different height layers has been found to be important at different stages of growth. Strong low-level shear, which might initially favor discrete cells with wider cold pools, promotes rapid organization of cells into a MCS through the merging of cold pools (e.g., Coniglio et al. 2010; Trapp et al. 2017). A shift from stronger low-level shear to stronger deep-layer shear as the MCS matures, especially for elevated convection, maintains cloud-layer shear, which is likely important for MCS maintenance (Coniglio et al. 2010). This wind shear can come from many sources, but the LLJ could play an important role specifically over the height layers where it is present. Additional studies are required to quantify the impact of LLJs on wind shear to better understand favorable environmental conditions for upscale growth.

Central Argentina is an ideal place to study convective upscale growth as it occurs over relatively small spatial and temporal scales compared to the U.S. Great Plains (Rasmussen and Houze 2016; Cancelada et al. 2020). In central Argentina, the Sierras de Córdoba (SDC) mountain range is a hot spot for terrain-focused upscale growth with no analog in the United States. Previously, simulations with relatively coarse resolution (>25-km grid spacing) have described the general synoptic ingredients associated with deep convection in central Argentina. The passage of midlevel troughs over the Andes mountains aids in the strengthening of the thermo-orographic northwest Argentinian low in the lee of the Andes (Seluchi et al. 2003; Rasmussen and Houze 2016), which in turn strengthens the South American low-level jet (SALLJ; Nicolini and Saulo 2000; Salio et al. 2002; Sasaki et al. 2022), bringing low-level moisture and heat southward into central Argentina (Rasmusson and Mo 1996; Nogués-Paegle and Mo 1997). This SALLJ is defined as warm, moist, northerly flow in these studies, and it is capped with cold, dry, subsiding air off the Andes, producing steep midtropospheric lapse rates (Rasmussen and Houze 2011, 2016) similar to the U.S. Great Plains. However, the extreme vertical extent of the Andes may lead to stronger leeside subsidence, both focusing the initiation of deep convection and keeping convection anchored to the terrain of the SDC during convective upscale growth (Rasmussen and Houze 2011, 2016).

Recently, the Remote sensing of Electrification, Lightning, And Mesoscale/microscale Processes with Adaptive Ground Observations (RELAMPAGO; Nesbitt et al. 2021) and Cloud, Aerosol, and Complex Terrain Interactions (CACTI; Varble et al. 2021) field campaigns took place near the SDC, providing the most extensive observations in this region to date. These observations, along with recent high-resolution simulations, have expanded the understanding of meso- and synoptic-scale ingredients favorable for convection near the SDC. Differences have been noted in storm environments in central Argentina compared to the United States. Environments with upscale growth of convection in Argentina are more likely characterized by larger convective available potential energy (CAPE) and weaker low-level vertical wind shear than the United States with likely influences from the SDC (Mulholland et al. 2018, 2019; Schumacher et al. 2021). Zhang et al. (2021) used a 6.5-month Weather Research and Forecasting (WRF) Model simulation covering the CACTI period and domain with 3-km grid spacing to show that MCSs preferentially initiated in regions of relatively low convective inhibition near and south of the SDC. Additionally, they showed rapid-growth MCSs are likely linked to strong low-level moisture transport and convergence resulting from the SALLJ; however, they did not objectively identify the SALLJ.

The SALLJ is a recurring feature during periods of upscale growth (Nicolini and Saulo 2000; Salio et al. 2002); therefore, it is prudent to understand its distribution and impacts. The highest frequency of the SALLJ shifts from Bolivia/Paraguay in austral winter to central Argentina in austral summer (Oliveira et al. 2018), possibly due to the poleward shift in baroclinicity (e.g., Garreaud 2000). This shift is also consistent with an increase in convective frequency near the SDC in austral summer (Rasmussen and Houze 2011). Using RELAMPAGO observations, Sasaki et al. (2022) found a wide variation in SALLJ height near the SDC. This variability in SALLJ temporal and spatial characteristics may result from the variety of mechanisms responsible for the presence of the SALLJ, from small-scale diurnal processes to pressure gradients in synoptic systems (Salio et al. 2002; Nicolini et al. 2004; Marengo et al. 2004; Wang and Fu 2004; Saulo et al. 2007; Sasaki et al. 2022). The most common SALLJs near the SDC last less than 2 days and peak overnight in the low levels; however, longer-duration periods (5–6 days) have elevated SALLJs that do not follow a diurnal cycle. These different types of SALLJs likely advect varying amounts of low-level moisture from distinct sources into the SDC region (Sasaki et al. 2022). However, details of the spatial variability of the SALLJ and its impact on the convective environment near the SDC are still uncertain and necessitate further study.

It is well documented that the SALLJ is generally associated with moisture and heat transport southward (e.g., Salio et al. 2002), but the evolution of the thermodynamic environment when the SALLJ is present has not been studied. Furthermore, vertical wind shear is inherent to LLJs so it is assumed that the SALLJ impacts environmental wind shear (e.g., Mulholland et al. 2019), but given the variability in the jet height it is not clear which vertical layers are affected. This variability in the height of wind shear may in turn affect convective upscale growth near the SDC. The complex terrain of the SDC has been shown in idealized studies to modify the large-scale flow, leading to areas of convergence near the mountains and a narrow band of strong vertical wind shear east of the ridgeline (Trapp et al. 2020;

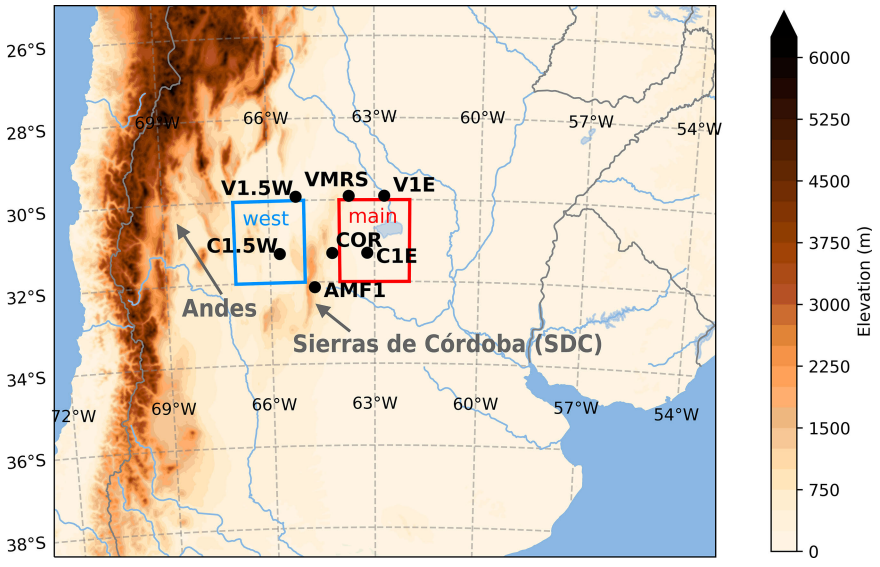

FIG. 1. Map of the WRF domain showing elevation (color shading), notable topographic features (gray text), and the locations (black text) and regions (colored boxes) where the impact of the SALLJ is quantified in this study. The locations shown are Córdoba (COR), Villa de María del Río Seco (VMRS), and Atmospheric Radiation Measurement Mobile Facility 1 (AMF1). An additional four locations are shown: 1.5°W and 1°E of both COR (C1.5W, C1E) and VMRS (V1.5W, V1E).

Mulholland et al. 2019). The flow may split around the SDC, leading to heterogeneities in the distribution of moisture and instability promoting convective initiation over sections of the SDC (Singh et al. 2022; Mulholland et al. 2019). However, these studies are limited to single cases in idealized model simulations and do not objectively identify the SALLJ or quantify its influence on these thermodynamic and dynamic conditions near the SDC.

This study uses the 6.5-month-long high-resolution WRF simulation described in Zhang et al. (2021) to quantify how the SALLJ spatially and temporally varies near the SDC and how the convective environment evolves when the SALLJ is present in this region. The 3-km grid spacing and hourly output from the WRF simulation allows for analysis of the spatial and temporal evolution of the SALLJ. Given the ability of similar resolution simulations to capture the shallow Great Plains LLJ (Smith et al. 2019), the WRF simulation is expected to reasonably capture the SALLJ. The specific objectives of this study are therefore to 1) evaluate WRF's ability to identify SALLJs and their known characteristics near the SDC, 2) explore the spatial and temporal variability of SALLJ, and 3) quantify changes in the convective environment in the vicinity of the SDC when the SALLJ is present.

2. Data sources

a. Model

To address our research objectives, a 6.5-month-long regional simulation was used to improve knowledge of the spatial and temporal variability of the SALLJ and its impacts on the convective environment. The WRF model (version 4.1.1; Skamarock et al. 2019) was run by the Atmospheric Research and Measurements group at the Pacific Northwest National Laboratory (PNNL) with 3-km horizontal grid spacing, 80 vertical levels, and hourly output. Initial and boundary conditions were obtained from the fifth-generation global reanalysis produced by the European Centre for Medium-Range Weather Forecasts (ERA5; Hersbach et al. 2020) with no observation or reanalysis nudging applied. The simulation covered the experimental period of the CACTI field campaign (15 October 2018–30 April 2019; encompassing the 6-week RELAMPAGO period), which occurred during the warm season for this region, an active period for MCSs. The WRF domain covered much of north and central Argentina including the RELAMPAGO study region near the SDC (Fig. 1). Model levels were stacked so that vertical grid spacing was 250 m or less below 5 km to better capture temperature inversions. The Mellor–Yamada–Nakanishi–Niino (MYNN) level-2.5 (Nakanishi and Niino 2006, 2009) eddy diffusivity mass flux and Thompson aerosol aware (Thompson and Eidhammer 2014) schemes were used to parameterize boundary layer processes and microphysical processes, respectively. Aerosol number concentrations for the microphysics scheme were nudged to the climatological dataset described in Thompson and Eidhammer (2014). Radiative transfer was parameterized using the Rapid Radiative Transfer Model for General Circulation Models (RRTMG; Iacono et al. 2008) with aerosol interactions turned on. The Noah land surface scheme (Tewari et al. 2004) is used with the Eta Similarity surface layer scheme (Monin and Obukhov 1954; Janjić 1994). More information can be found in Zhang et al. (2021). The variables used in this analysis are three-dimensional winds, simulated column-maximum reflectivity, 850-hPa specific humidity, and maximum CAPE (calculated for the average parcel in a 500-m layer centered around the maximum theta-e in the lowest 3000 m, including the virtual temperature correction; Ladwig 2017).

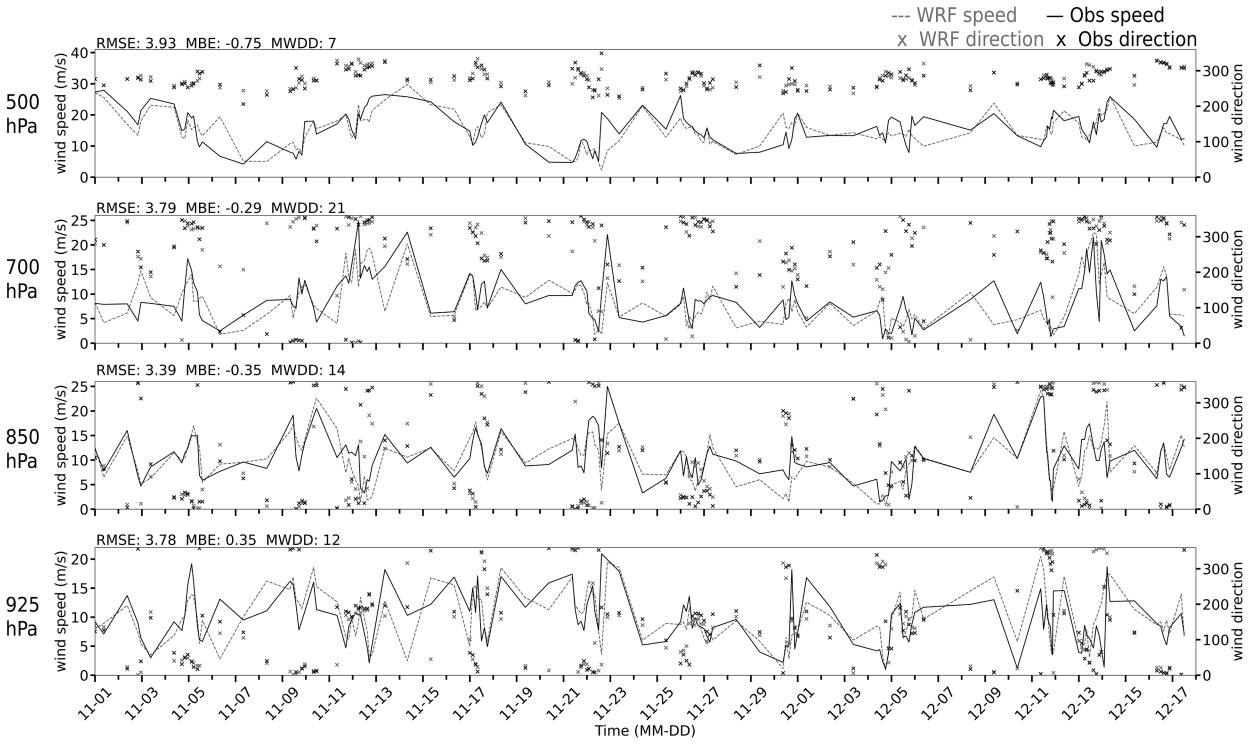

FIG. 2. Time series of wind speed and direction at various pressure levels for WRF (gray) and observations (black) during the RELAMPAGO period at VMRS. Statistical parameters of root-mean-square error (RMSE), mean bias error (MBE), and median wind direction difference (MWDD) are shown.

b. *RELAMPAGO fixed soundings*

Soundings launched at two fixed sites during the RELAMPAGO field campaign (1 November–17 December 2018; UCAR/NCAR–Earth Observing Laboratory 2020) were used to evaluate the ability of the WRF simulation to adequately reproduce the SALLJ. The operational site at Córdoba (COR; 31.2988°S, 64.2128°W; elevation: 490 m) is just to the east of the SDC while Villa de María del Río Seco (VMRS; 29.9068°S, 63.7268°W; elevation: 341 m) was a temporary RELAMPAGO location ~175 km north-northeast of COR (Fig. 1). Throughout the campaign soundings were launched at COR at least twice a day and at least once a day at VMRS, with higher frequency launches (at least every 3 h) during intensive observational periods. This led to a total of 175 soundings at COR and 136 at VMRS. SALLJs and their characteristics (height, timing, strength) were quantified using the winds from these soundings following a similar method to Sasaki et al. (2022). Information on the quality control procedures and radiosonde specifications can be found in the dataset documentation (UCAR/NCAR–Earth Observing Laboratory 2020).

3. Evaluation of WRF simulation and identification of SALLJ periods

Before exploring the characteristics and impacts of the SALLJ, the ability of WRF to capture LLJs was evaluated by comparing the WRF output against sounding observations from the RELAMPAGO field campaign. Comparisons of the wind speeds and directions at COR and VMRS at various height levels indicate that the WRF-simulated winds reasonably capture the flow near the SDC (Figs. 2 and 3). The root-mean-square errors (RMSE) of wind speeds at these locations are roughly 3–5 m s^{-1} and the median wind direction differences (MWDD) are small (<23°). Minimal mean bias errors (MBE; $<\pm 1$ m s^{-1}) are found at most levels. The largest biases (~ -2 m s^{-1}) are found in the low levels at COR, indicating that low level winds close to the higher terrain may be slightly underestimated in WRF (Fig. 3).

Given the generally good agreements in winds, but the slight underestimation near the higher terrain of the SDC, we further explored the ability of WRF to identify LLJs at the same time as those in observations at the two stations. Sasaki et al. (2022) modified previous LLJ identification criteria to capture LLJs in central Argentina. Their criteria are: 1) a wind maximum > 12 m s^{-1} within 3200 m AGL and 2) a decrease > 6 m s^{-1} from maximum to first minimum or 5700 m AGL. When the criteria from Sasaki et al. (2022) are applied to both the soundings and the WRF output, a LLJ is identified in the WRF output in two thirds of the times compared to jets identified in sounding data (Table 1). This result is an improvement from ERA5 which identified LLJs half of the times (Sasaki et al. 2022). The criteria in Sasaki et al. (2022) were optimized for observational data; however, it is known that simulations (including this simulation) tend to miss wind

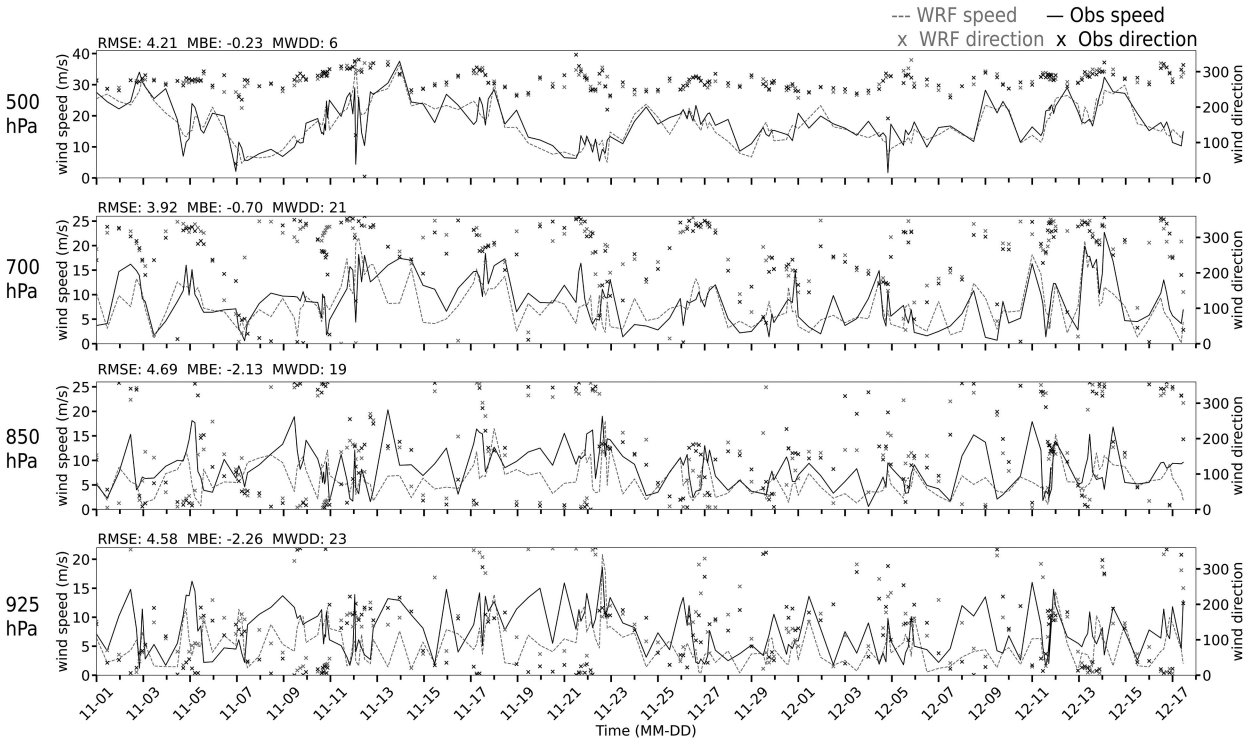

FIG. 3. As in Fig. 2, but for the COR sounding site.

maxima and minima (whether due to physics or required smoothing; e.g., Walters et al. 2014). Relaxing the maximum (from 12 to 10 m s^{-1}) and the minimum (from 6 to 4 m s^{-1}) wind speed in the criteria, the WRF simulation reproduces 80% of the jets found in the sounding data (Table 1). These relaxed criteria will be therefore used for further analysis of LLJs in this study.

To confidently expand the characterization of the SALLJ in time and space, it is important that the simulation not only identify LLJs at the correct times, but that the simulated jets have similar characteristics to those found in observations. Distributions of the pressure level and wind speed at the jet core from WRF and observational soundings are shown in Fig. 4. The purpose here is to compare the simulated and observed distributions; a physical explanation of the frequencies can be found in Sasaki et al. (2022). The overall shapes of the distributions are similar between the WRF output and the soundings, illustrating that the frequency of shallow and elevated jets are similar in observations and the simulation. The frequency of shallow LLJs close to the SDC (e.g., at COR) is slightly lower in WRF than in the observations, likely due to the underestimation of the winds near the higher terrain. However, the accuracy of the winds, LLJ identification, and LLJ characteristics provide confidence that the WRF simulation can be used to infer characteristics of the SALLJ.

TABLE 1. Number of LLJs identified at VMRS and COR for WRF and RELAMPAGO observations using the Sasaki et al. (2022) criteria and a relaxed version.

	Sasaki et al. (2022) criteria		Relaxed criteria	
Station	Obs	WRF	Obs	WRF
VMRS	84	53	103	88
COR	64	44	88	64

Last, continuity criteria were introduced using the continuous spatial information provided by WRF to allow for the objective definition of SALLJ periods, which are helpful for identifying whether a certain time period is impacted by the SALLJ. These SALLJ periods were defined using the proportion of the region (colored boxes in Fig. 1) meeting the relaxed LLJ criteria over a period of time where the SALLJs are those LLJs with a northerly meridional component greater than or equal to the zonal component. The criterion for the start of a SALLJ period is SALLJ coverage $\geq$ 30% for 2 or more consecutive hours and the criterion for the end of a SALLJ period is SALLJ coverage $<$ 30% for $>$24 consecutive hours. Time periods outside of these *SALLJ periods* are defined as *non-SALLJ periods*. The results from applying these criteria are shown for an example period for the main SDC region (Fig. 5), where most of the RELAMPAGO observations were taken, with the gray shading showing the SALLJ periods. The 30% (dashed line; similar to Du et al. 2014) and 24-h thresholds highlight active jet periods, hereafter called *SALLJ periods*, and account for any noise in the application of the objective criteria to hourly data and for diurnal cycles in SALLJ strength. A total of 33 SALLJ periods were identified with a strong skew toward those lasting less than 2 days (not shown), similar to past work (Salio et al. 2002; Sasaki et al. 2022).

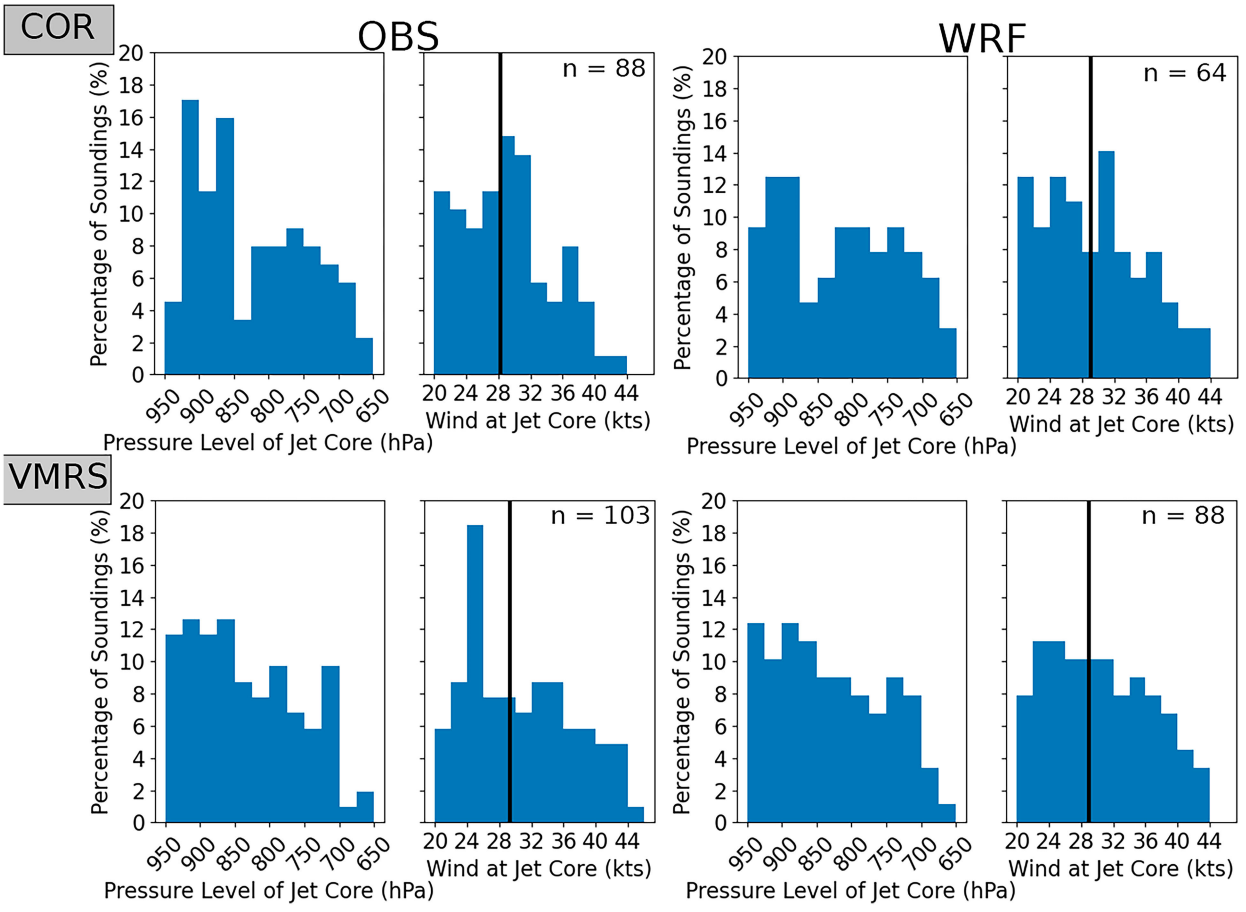

FIG. 4. Probability distributions of LLJ core wind speed and the pressure level at which peak winds occurred for COR and VMRS in RELAMPAGO observations and in WRF. The black lines are median jet core wind speeds.

4. Spatial and temporal distributions of the SALLJ

a. Horizontal distributions of SALLJ occurrence

Using spatially continuous high-resolution WRF output, spatial variability is found in SALLJ frequency near the SDC. Figure 6 shows the horizontal distribution of the occurrence of SALLJs in 2-month composites for late spring through midfall (i.e., covering the entire period of the WRF run). Within the WRF domain, the SALLJ is most frequently found in the vicinity of the SDC, with maxima to the west and north of the SDC, a secondary maximum to the east of the SDC, and frequency decreasing eastward over the plains. Overall, similar patterns are found for the whole period, but by the fall, the maxima on either side of the SDC decrease slightly and the frequency of the SALLJ eastward decreases faster.

The spatial and temporal maxima in SALLJ frequency from WRF are in good agreement with past studies (Oliveira et al. 2018; Salio et al. 2002); however, the horizontal resolution

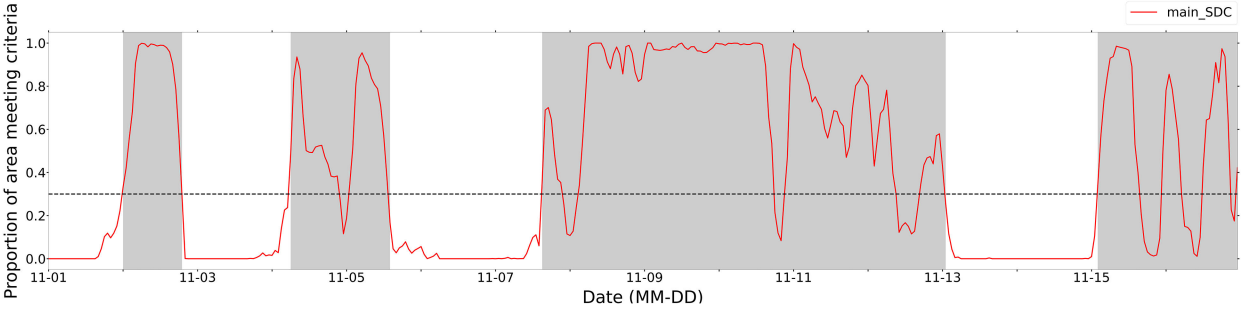

FIG. 5. Example period showing how the proportion of the area meeting the relaxed SALLJ criteria (red line) is combined with time continuity criteria to define SALLJ periods (gray shading) in the main SDC region.

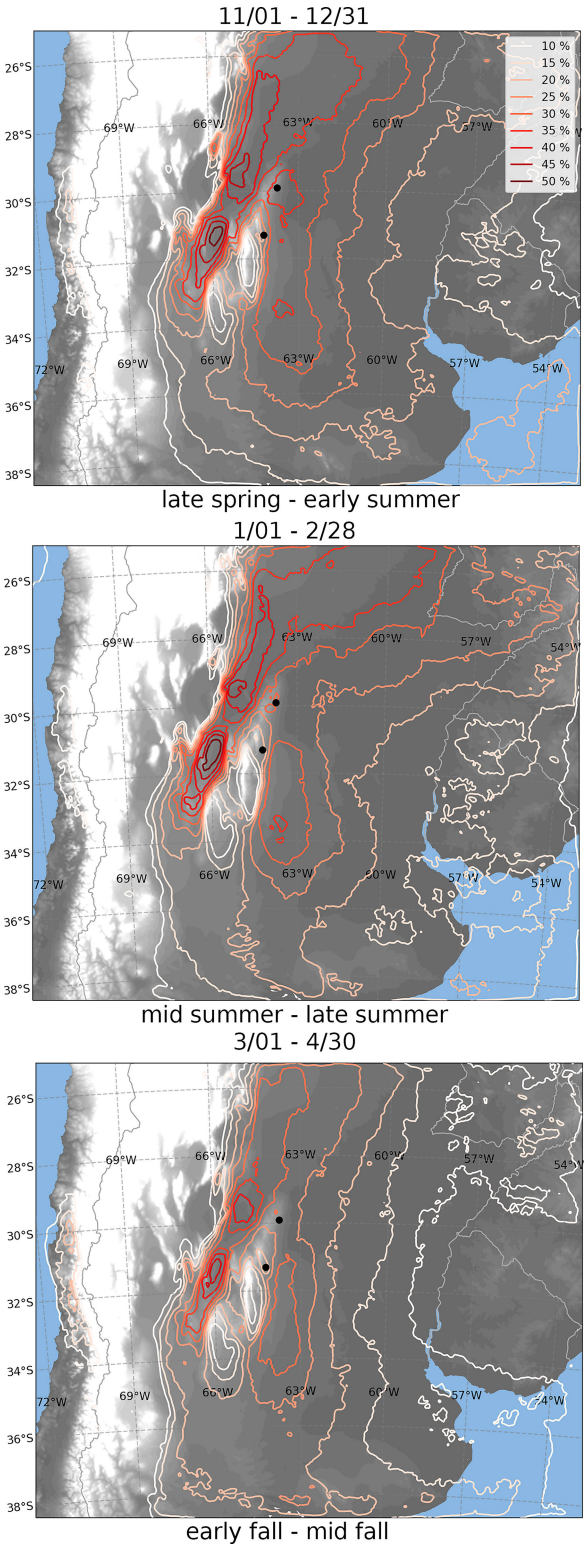

FIG. 6. Two-month maps of SALLJ frequency (color contours) in the WRF domain. The elevation is shown in the grayscale shading with white being the highest elevation.

(>0.5°) of the reanalysis data used in those studies did not allow for identification of maxima/minima near the SDC. The maxima west of the SDC may be the result of channeling between ridges on the eastern edge of the Andes and the SDC (Campetella and Vera 2002). Minima in SALLJ frequency are found over the higher terrain of the SDC and extend into areas where the terrain appears to block northerly flow. This result is consistent with Singh et al. (2022), who used an idealized simulation to show a case where, from a Froude number perspective, flow was unable to ascend the ridge and instead split around it. The Froude number was calculated using Fr = U/Nh, where U and N are average values between the ground and ridgetop for northerly wind speed and the Brunt–Väisälä frequency, respectively, and h is the height of the crest (~2000 m) (Reinecke and Durran 2008). Following this methodology, 94% of SALLJ times in the WRF simulation had a Froude number less than 1 (blocking) at VMRS. This generalizes their result that during most SALLJ times flow is blocked and splits around the SDC.

b. *Temporal distributions of SALLJ occurrence*

To investigate diurnal cycles in SALLJ frequency and the temporal variability near the SDC, Fig. 7 shows frequency distributions of SALLJs by hour. WRF SALLJ frequency distributions are shown for the three fixed RELAMPAGO-CACTI sounding locations close to the SDC (VMRS, COR, and AMF1), as well as additional locations within the regions of highest SALLJ frequency (Fig. 6) away from the SDC (Fig. 1): 1° to the east and 1.5° to the west. Considering all SALLJs, the highest frequencies are found overnight for all locations, matching RELAMPAGO observations at VMRS and COR (see Fig. 7 of Sasaki et al. 2022). Specifically, a similar broad peak from 0300 to 1200 UTC is found at VMRS (Fig. 7a) and a narrower, sharp peak from 0100 to 0600 UTC is found at COR (Fig. 7b). The frequencies of SALLJs at each hour in WRF are lower than those in observations (Fig. 7 of Sasaki et al. 2022); however, the WRF data are more comprehensive as the observational soundings were preferentially launched during forecasted active SALLJ periods and over a shorter time period than WRF.

Comparing the frequency of shallow (blue) and elevated (red) SALLJs provides insight into possible mechanisms responsible for the SALLJ and helpful context when exploring the impact of the jet (Fig. 7). A 1750 m AGL (~825 hPa) threshold was chosen to differentiate between shallow and elevated SALLJs as it is an approximate delineation between jet core groupings found in observations and WRF (Fig. 4). When broken down by height, differences are seen between the highest elevation locations (COR and AMF1) and the other locations. At VMRS and the locations away from the SDC (Figs. 7a,c–f), the most frequent shallower SALLJs have a strong overnight skew, while the elevated jets are more equally spread throughout the day. The slight afternoon skew in elevated jets might be due to some boundary layer LLJs at the top of a deep mixed layer (Carroll et al. 2019) being classified as elevated jets. The distributions at COR (Fig. 7b) are different, with the shallower SALLJs having a slight evening rather than overnight skew but, importantly, are much less frequent. AMF1 (Fig. 7g) is the highest elevation location and SALLJs are much

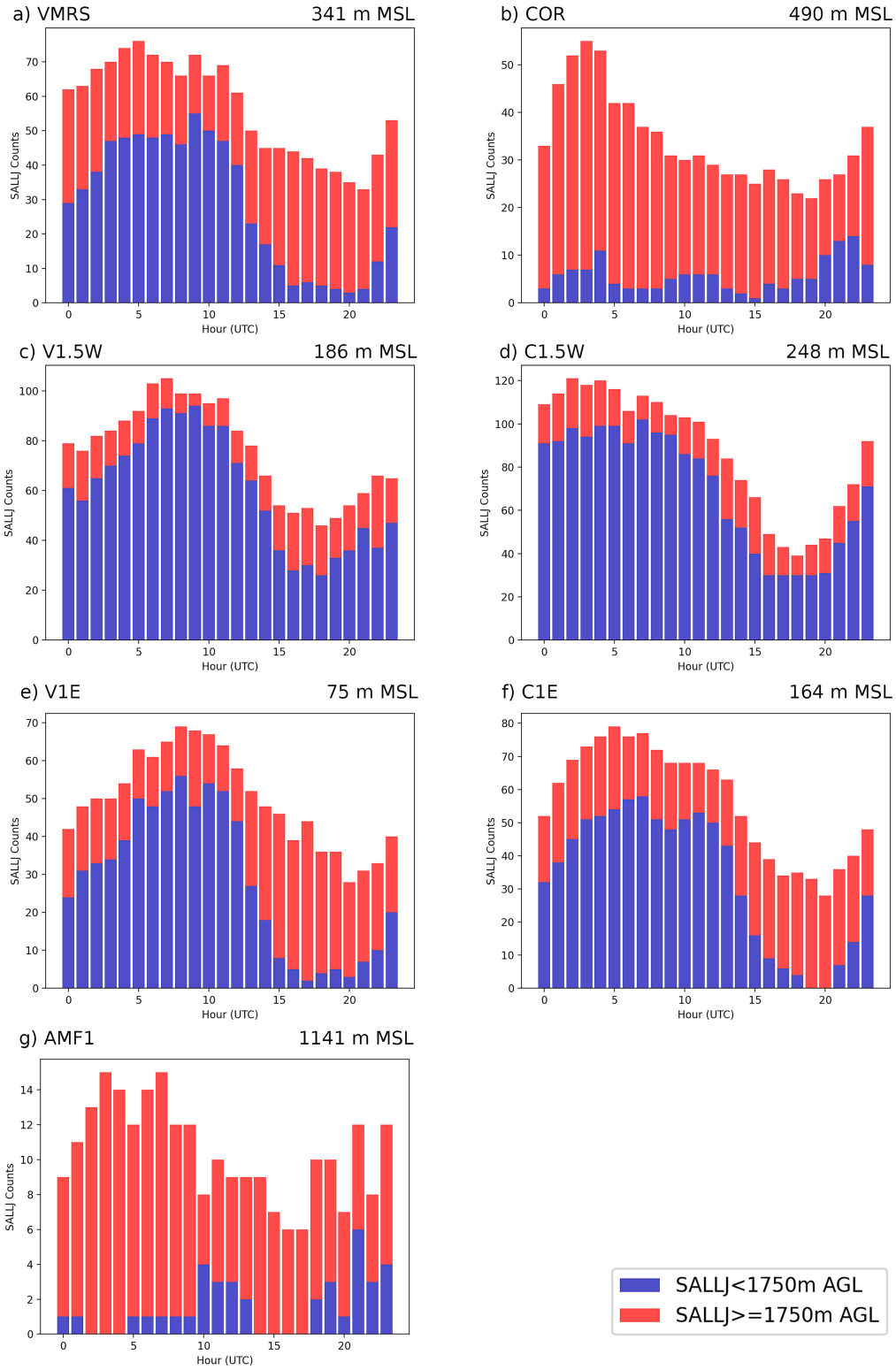

FIG. 7. Stacked histograms of SALLJs by hour for jets peaking below (blue) and above (red) 1750 m AGL at locations shown in Fig. 1 for (a) VMRS, (b) COR, (c) V1.5W, (d) C1.5W, (e) V1E, (f) C1E, and (g) AMF1. Note that local time is UTC − 3 h.

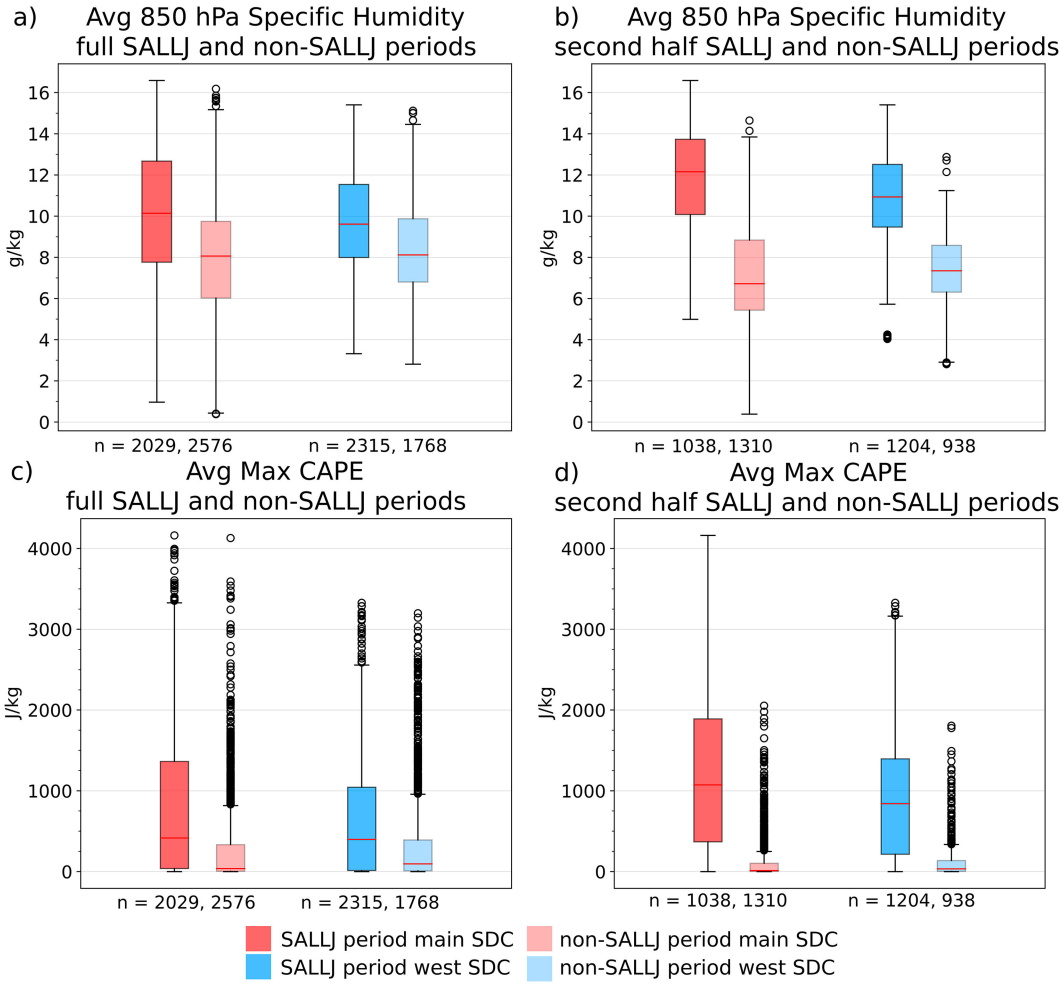

FIG. 8. Boxplots of specific humidity and CAPE values averaged over the main (red) and west (blue) SDC regions during (a),(c) all SALLJ and non-SALLJ periods and (b),(d) the second half of the SALLJ and non-SALLJ periods. The box extends from the first to third quartiles of the data, with a red line at the median. The whiskers show the range of the data up to 1.5 times the interquartile range. Points outside that are shown as outliers (black dots).

less frequent (<15 at any hour) than any other location with few shallow jets. As mentioned earlier, the SALLJ often splits around the SDC which aligns with the general lower frequencies at COR and AMF1. When SALLJs are found over the higher terrain of the SDC they are more elevated. The elevated jets at COR have an overnight skew resembling the shallower jets at the lower-elevation locations, suggesting that these jets may still be diurnally driven. The height at which the SALLJ peaks is important not only for understanding the mechanisms responsible for the jet but also for understanding its impact on the convective environment.

5. SALLJ effects on the thermodynamics and dynamics of the convective environment

Moisture, instability, lift, and wind shear all determine if convective storms form, their characteristics, and if convective upscale growth occurs. To investigate the impact of the SALLJ on these environmental conditions, the distributions of these variables are compared for SALLJ and non-SALLJ periods. Additionally, comparisons are made between regions (boxes in Fig. 1) to determine if and how these conditions vary around the SDC.

a. Specific humidity and CAPE

Specific humidity at 850 hPa and maximum CAPE are useful metrics for low-level moisture and instability, which are necessary ingredients for convective storms. The median 850-hPa specific humidity and CAPE magnitudes are higher during SALLJ periods than non-SALLJ periods for both the west and main SDC regions, but there is a wide range of values (Figs. 8a,c). The impacts of the SALLJ are not instantaneous and thus moisture and CAPE change with time, increasing while the SALLJ is present. Therefore, we also consider the second half (based upon the length of each period) of the SALLJ and non-SALLJ periods to account for this time delay (Figs. 8b,d). The differences between SALLJ and non-SALLJ periods become larger

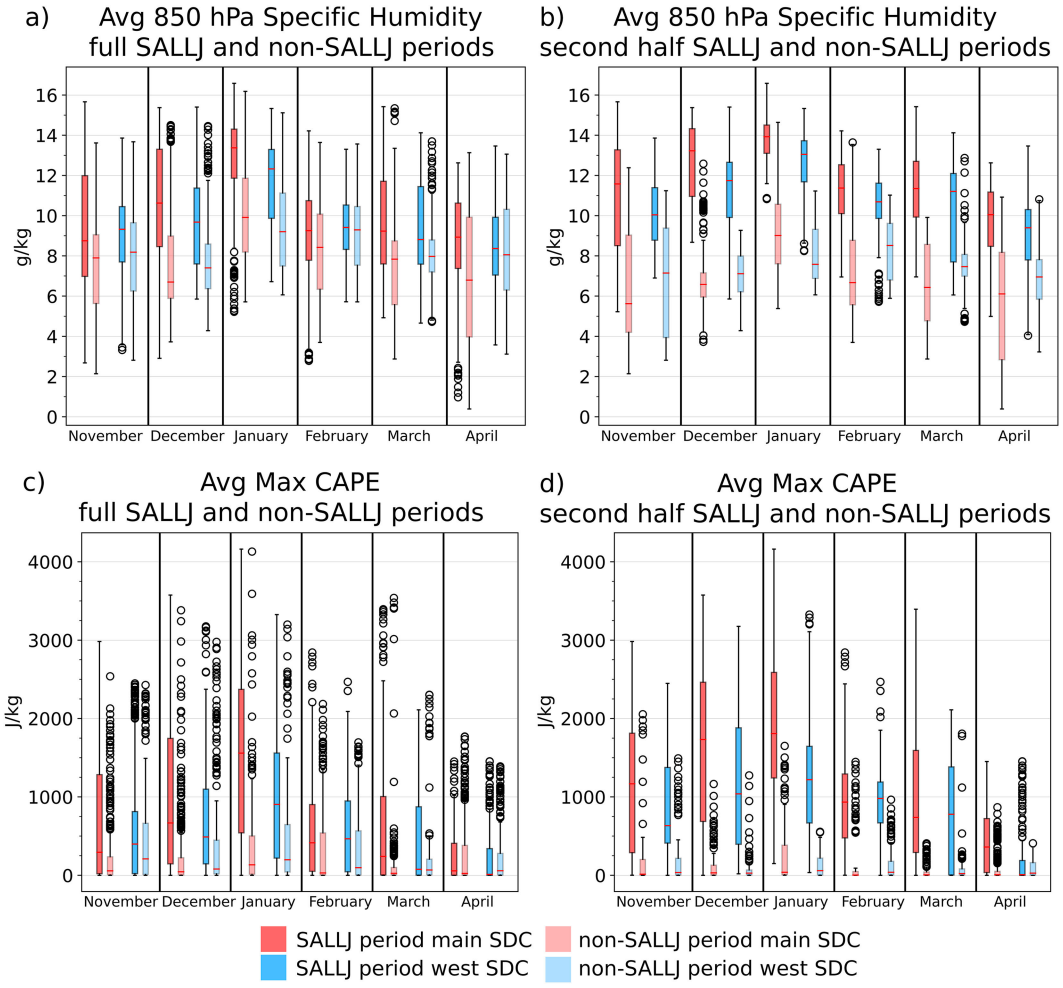

FIG. 9. As in Fig. 8, but broken down by month.

(~2–3 times) when comparing the second half of these periods. The higher amounts of moisture and CAPE during the second half of SALLJ periods than during the full SALLJ periods show that moisture and low-level heat (leading to instability) increase when the SALLJ is present. The lower amounts of moisture during the second half of non-SALLJ periods than during the full non-SALLJ periods show that moisture decreases during non-SALLJ periods. This time lag may help explain widespread convection occurring near the end or just after SALLJ periods in both this model run (not shown) and observations (Sasaki et al. 2022). Magnitudes of CAPE and low-level moisture that could support deep convection are still found during some non-SALLJ periods, but are less frequent than during SALLJ periods.

Differences in median values of specific humidity and CAPE between SALLJ and non-SALLJ periods are 24% and 34% smaller, respectively, in the west SDC region than in the main SDC region. Jet properties (peak wind, specific humidity, and duration) are similar between the regions (not shown); therefore, the variation in the SALLJ's impact likely results from different spatial patterns of SALLJ frequency over the two regions (Fig. 6) leading to broader jet coverage within the main SDC region compared to the west. Specifically, the SALLJ is found to cover at least 65% of the region in about half of the SALLJ times in the main SDC region compared to only about a quarter of SALLJ times for the west SDC. Additionally, jet height does not always align with the level of peak moisture or the parcel height used for CAPE calculations. The vertical structure of the jet, moisture, and instability may all contribute to differences in jet impacts between the regions and deserve further attention in future research.

Similar differences in CAPE and specific humidity between SALLJ and non-SALLJ periods are found on monthly time scales, with some variability (Fig. 9). December and January stand out as having the largest differences between SALLJ and non-SALLJ periods (Figs. 9a,c), especially when considering only the second half of the jet periods (Figs. 9b,d). These differences are larger than those found in the 6-month medians (Fig. 8). CAPE values have a large spread and part of the motivation of the monthly breakdown was to determine when the high values of CAPE during non-SALLJ periods

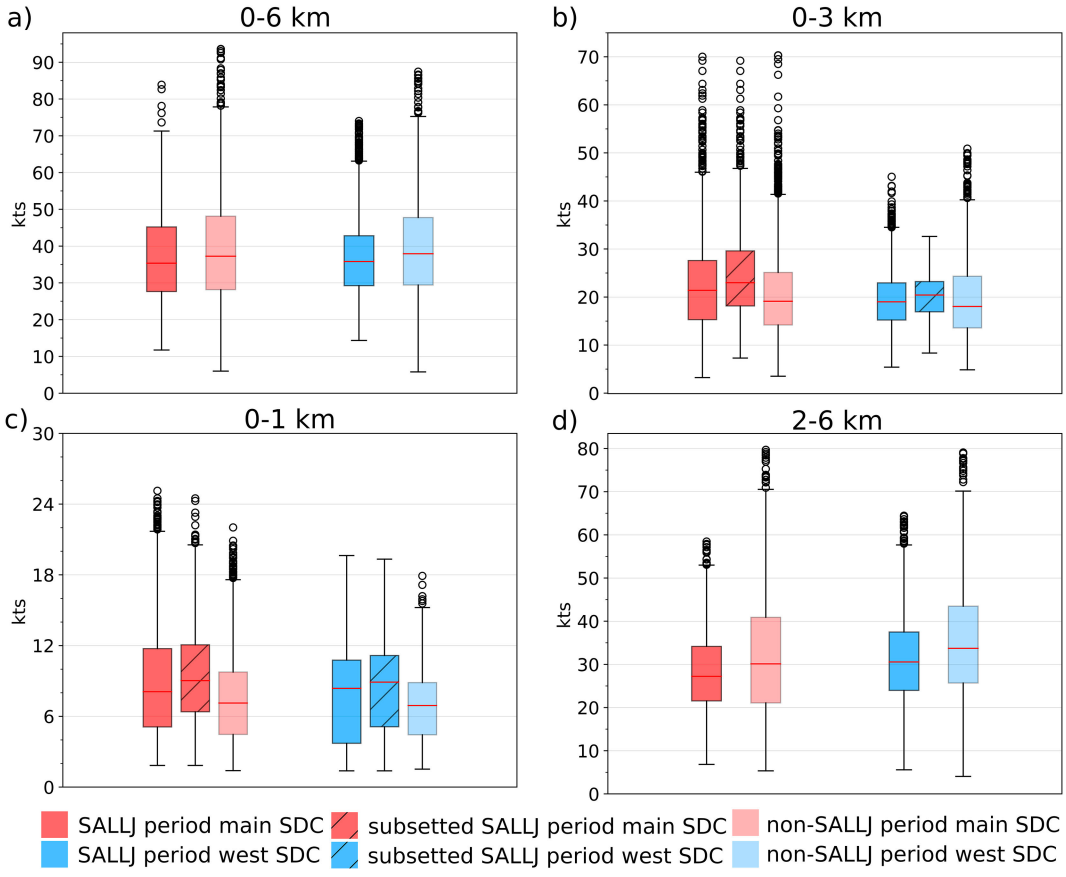

FIG. 10. Boxplots of the magnitudes of wind shear during SALLJ and non-SALLJ periods averaged over the main (red) and west (blue) SDC regions for (a) 0–6, (b) 0–3, (c) 0–1, and (d) 2–6 km. Subsetted SALLJ periods (hatched) are times when the SALLJ height is near the top of the calculated shear layer (0.5–1.5 km for 0–1 km and >2.5 km for 0–3 km).

occurred. As expected, the highest values (>2500 J kg^{-1}) often occur in December, January, and February (summer), but high values are also found more broadly throughout different months in the warm season.

b. *Magnitude of wind shear*

Previous studies (e.g., Mulholland et al. 2019; Singh et al. 2022) mention that the SALLJ by definition enhances vertical wind shear magnitudes and thus creates favorable environments for the organization of convection. However, quantifying the impact through objectively identifying the SALLJ shows that their generalizations may not be valid and that the relationship is more nuanced. The magnitude of the wind vector differences (WVDs) were calculated over fixed height layers commonly used in the literature to relate to convective organization (e.g., Coniglio et al. 2010; Dial et al. 2010; Schumacher et al. 2021). WVD is similar to vertical wind shear but is in units of wind speed to make interpretation easier. The term "shear" is used in this text as WVDs are calculated over fixed height layers. In general, differences in the magnitude of wind shear over any fixed layer between SALLJ and non-SALLJ periods (Fig. 10) are small, with median wind shear differences less than 10% except for 0–1 km where median shear is 13% and 21% higher in the main and west SDC regions, respectively, during SALLJ periods.

The lack of a relationship between the presence of the SALLJ and wind shear could partially be a result of the known variability in jet height (Fig. 4; Vera et al. 2006; Sasaki et al. 2022). To test whether the variability in jet height could be masking the impact of the SALLJ on low-level shear, the hatched box plots (Figs. 10b,c) show the 0–1- and 0–3-km shear values during the subset of SALLJ times when the SALLJ peak height is near the top of the shear layer (i.e., 0.5–1.5-km jet peak height for 0–1-km shear, >2.5-km jet peak height for 0–3-km shear). The median shear in these subsetted SALLJ periods is slightly (1–2 kt; 1 kt ≈ 0.51 m s^{-1}) increased from all SALLJ periods. This increase results in differences in median values between non-SALLJ and subsetted SALLJ periods of 14%–20% for 0–3-km and 26%–29% for 0–1-km shear. In a relative sense, these differences are about twice as large as those between all SALLJ and non-SALLJ periods, but all differences are <4 kt. Accounting for jet height amplifies wind shear magnitudes during SALLJ periods, but SALLJ height variability does not completely explain similar wind shear values between SALLJ

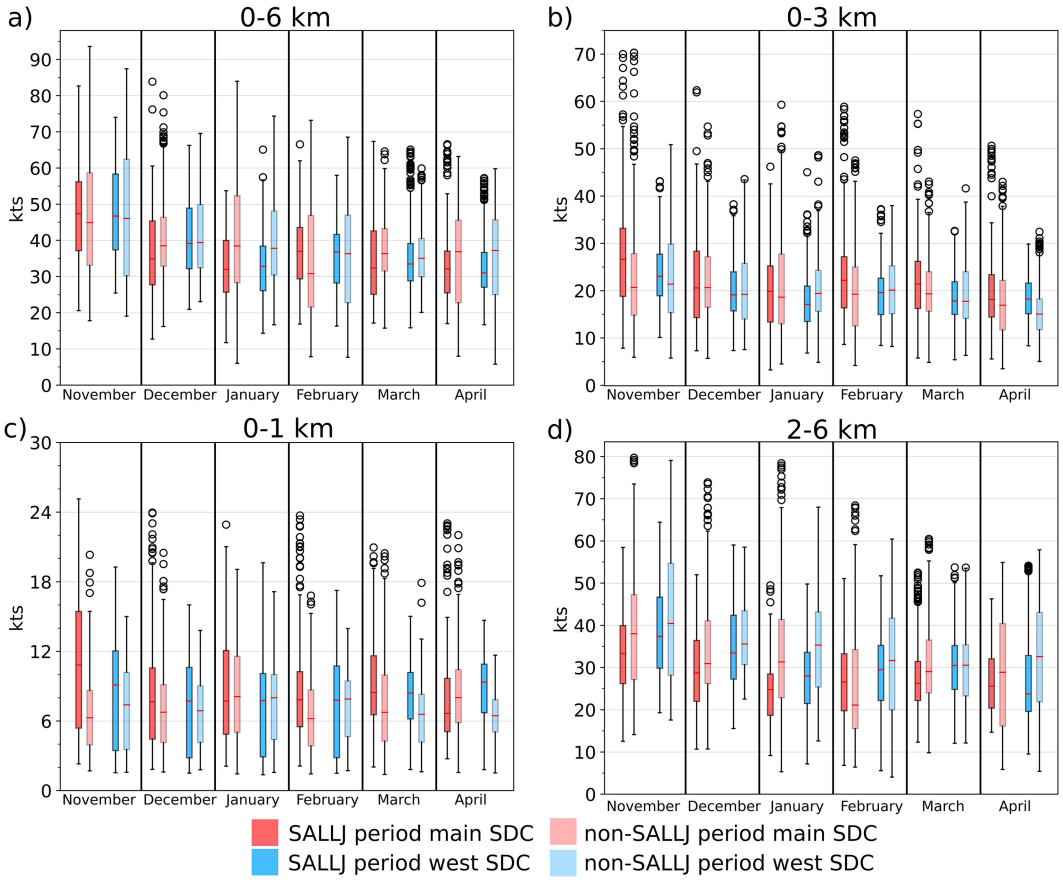

FIG. 11. As in Fig. 10, but broken down by month.

and non-SALLJ periods. The moderate values of wind shear (~20 kt for 0–3 km) during non-SALLJ periods indicate that there are mechanisms other than the SALLJ that facilitate production of low-level wind shear in this region. Mesosynoptic dynamics common in the region, such as diurnally driven flows (Singh et al. 2022) or strong westerly flow aloft during synoptic activity (Piersante et al. 2021), may produce enhanced wind shear in the absence of the SALLJ. However, the SALLJ can amplify wind shear magnitudes, particularly over height ranges that account for the height at which the jet peaks.

While the differences between SALLJ and non-SALLJ periods are small, deep-layer shear varies seasonally. Overall, the 6-month median 0–6-km shear is around 35 kt (Fig. 10a), but the highest median values (~45 kt) are found in late spring (November) with lower values in the summer and fall (Fig. 11a). A similar pattern is seen in 2–6-km shear values, with little seasonal variation in the 0–1- and 0–3-km values. The higher values of deep-layer shear in the spring may be related to the increased seasonal synoptic activity (Piersante et al. 2021).

c. *Wind shear direction*

The direction of wind shear relative to the zone of low-level forcing is important for convective organization as it influences the advection of hydrometeors and the residence time of storms within this zone of forcing (e.g., Dial et al. 2010). Figure 12 shows comparisons of hodographs during SALLJ and non-SALLJ periods for the main and west SDC regions. These hodographs suggest a limited impact on shear magnitudes from the SALLJ, but a clear impact on directional shear. The mean hodographs (color solid outlined) for SALLJ periods show a clear SALLJ signal in the low-level winds compared to the non-SALLJ periods. The SALLJ periods have low-level winds from the north-northeast and more anticyclonic low-level curvature than the non-SALLJ periods. The magnitudes of 0–1- and 0–3-km shear in the mean hodographs are slightly larger during SALLJ periods than non-SALLJ periods. For 0–1 km the differences are moderate (5–7 kt) but for 0–3 km these differences are greatly reduced (<3 kt). The difference in the result compared to the shear magnitude box plots (Fig. 10) can be explained in terms computing arithmetic (Fig. 10) versus vector (Fig. 12) spatial means. This highlights that the direction of low-level shear is highly variable in non-SALLJ situations, but much more consistent in SALLJ situations. In the WRF simulation, MCS tracks (i.e., Fig. 14 in Zhang et al. 2021) reveal a typical propagation direction of east-northeast. Therefore, the low-level inflow to these MCSs would be stronger with SALLJ winds than non-SALLJ winds. Similar low-level curvature was noted in supercell environments in central Argentina (Piscitelli et al. 2022),

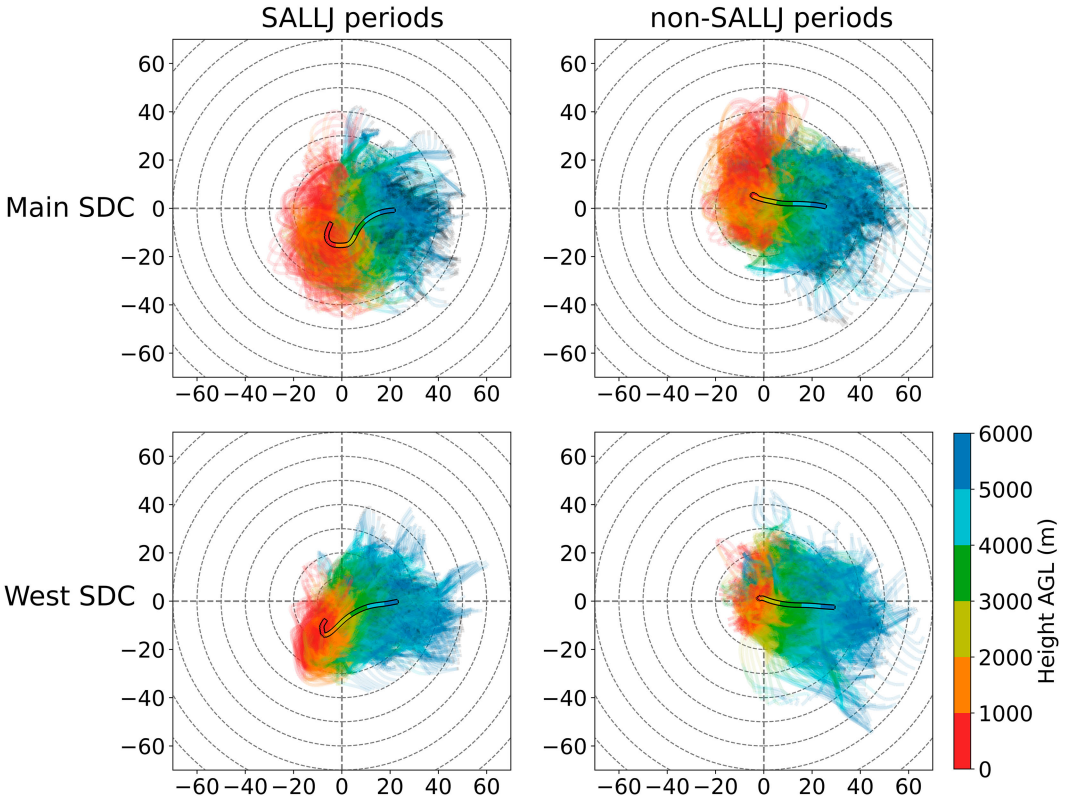

FIG. 12. All (color shaded) and mean composite (color solid outlined) hodographs for (left) SALLJ and (right) non-SALLJ periods averaged over the (top) main and (bottom) west SDC regions.

suggesting an important role of the SALLJ in convective evolution.

To further understand how the SALLJ may orient cloud-layer shear in a favorable direction relative to initiating boundaries (e.g., Coniglio et al. 2010), Fig. 13 shows comparisons of 2–6-km ("cloud-layer") wind shear vectors during non-SALLJ and SALLJ periods. Two RELAMPAGO sounding locations close to the SDC are shown (Figs. 13a,b), as well as locations farther from the SDC (1° to the east; Figs. 13c,d), to determine if wind shear direction varies relative to the SDC. For 2–6 km, the shear vector during non-SALLJ periods is oriented from a westerly direction at all locations close to and away from the SDC. During SALLJ periods, the 2–6-km shear is oriented instead in a southwest direction at all locations. Strong northerly winds from the SALLJ in the low levels coupled with westerly winds in the upper levels lead to a shear vector with more of a southerly component during SALLJ periods. In cases where the SDC is acting as the low-level forcing, orienting the cloud-layer wind shear parallel to this boundary (N-S orientation) could increase the rate of upscale growth (Dial et al. 2010; Mulholland et al. 2019). In terms of the magnitude of 2–6-km shear, the SALLJ periods at stations close to the SDC (COR and VMRS; Figs. 13a,b) have a higher frequency of large values (yellow, orange, red) than the stations further from the SDC (Figs. 13c,d). This may be related to the higher frequency of elevated jets near the SDC (Figs. 7a,b).

The distributions of wind shear magnitude and direction during SALLJ periods highlight complexities in relating the SALLJ and favorable dynamic environments. SALLJ periods are associated with increased moisture and instability, low-level curvature favorable for organized convection, and an orientation of cloud-layer wind shear parallel to the terrain of the SDC that often serves as the initiation source. The SALLJ can also amplify low-level wind shear magnitudes (particularly when accounting for the jet height); however, amplification is somewhat limited due to the presence of speed shear in most conditions.

6. Case study: 29–30 January 2019

The impact of the presence of the SALLJ on the dynamic environment is complicated in an aggregate sense and thus motivates investigating if and in which cases the SALLJ has a clearer impact. To this end, the case study of 29–30 January 2019 is shown where the SALLJ is present over an extended period prior to the upscale growth of convection near the SDC (in both the west and main SDC regions). This case was chosen for further analysis because deep convection initiates over the SDC and grows upscale into an MCS in that same region. Additionally, the composite box plots from January show a strong signal of the SALLJ's impact on the thermodynamic environment (Fig. 9), but an unclear impact on the dynamic environment (Fig. 11).

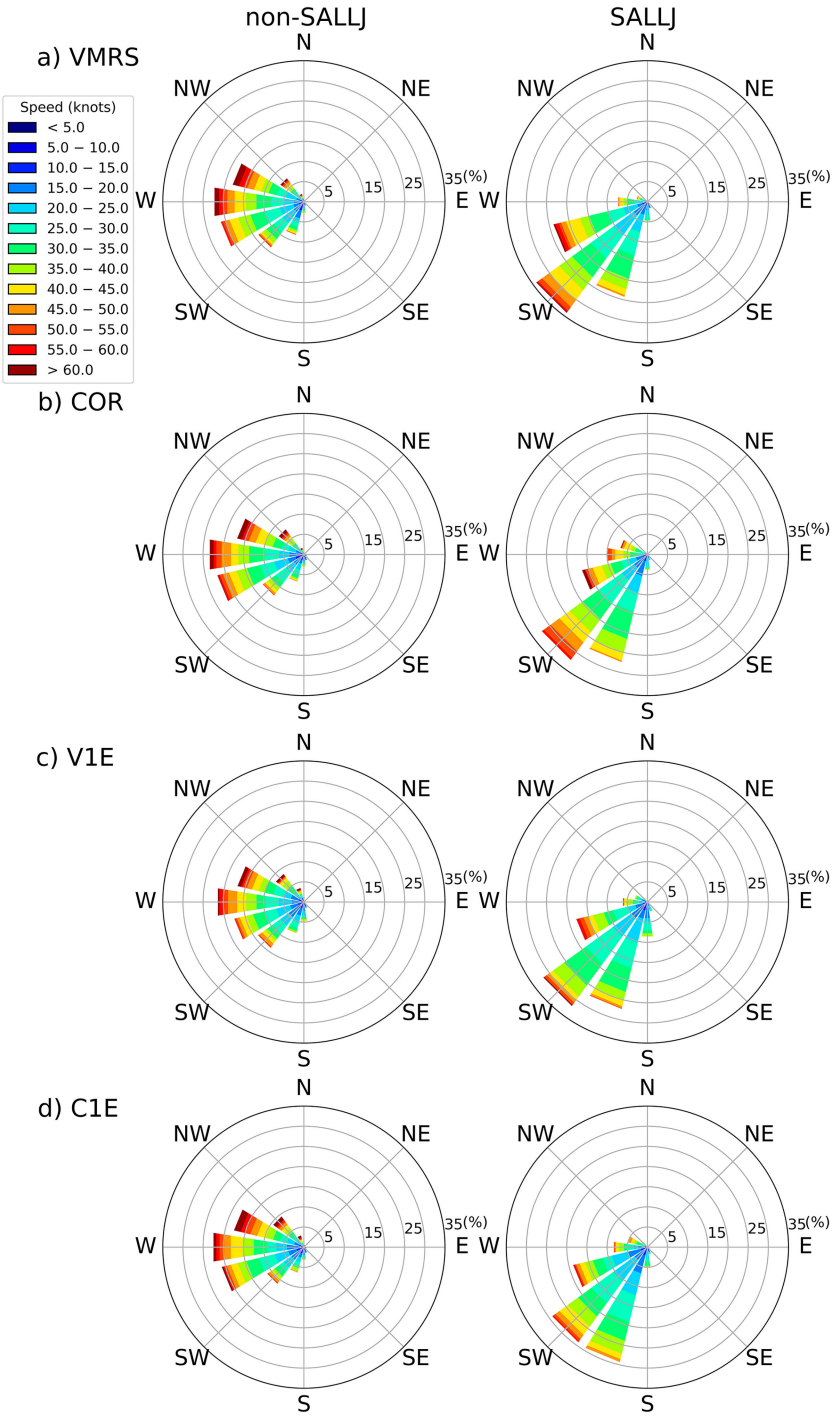

FIG. 13. Wind roses of 2–6-km wind shear vectors during non-SALLJ and SALLJ periods for (a) VMRS, (b) COR, (c) V1E, and (d) C1E. Percentage frequency is marked in 5% intervals with every other mark labeled.

Figures 14 and 15 show spatially averaged values of environmental variables in the main and west SDC regions, respectively, along with SALLJ identification (red stars) and SALLJ periods (gray shading). To give context, the longer period from 20 to 30 January is shown when the SALLJ is generally present, fluctuating in coverage and intensity. There was a break in the SALLJ period on 26 and 27 January in the main SDC region (Fig. 14) but not in the west (Fig. 15).

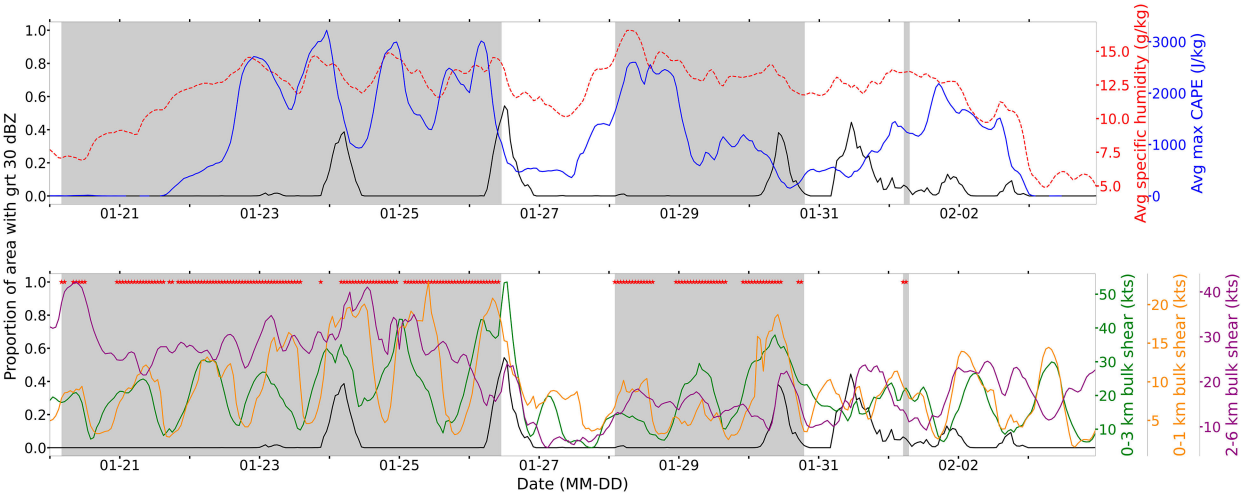

FIG. 14. Time series of spatially averaged values of environmental variables along with SALLJ identification (red stars), SALLJ periods (gray shading), and >30-dBZ simulated reflectivity coverage (black line) in the main SDC region. The environmental variables shown are 850-hPa specific humidity (red dashed line), maximum CAPE (blue line), and the magnitude of 0–1- (yellow line), 0–3- (green line), and 2–6-km (purple line) vertical wind shear.

In both regions there was a distinct increase in specific humidity (red dashed line) from 20 to 22 January with high values (>12 g kg^{-1}) lasting through the start of February. There was a slight drop in specific humidity on 26 January with a rebound on 27 January, coinciding with the longest break in the SALLJ during this period. CAPE (blue line) follows a similar pattern with larger fluctuations and steep drops during the periods with the most widespread simulated convection (black line). High-frequency fluctuations are found in 0–1- and 0–3-km wind shear which often vary similarly together, but for all layers a large spread in values is found when the SALLJ is present (Figs. 14 and 15).

Focusing on 29–30 January when convection grew upscale over the SDC (i.e., was widespread; black line), high-resolution spatial maps are shown from 1800 UTC 29 January to 0900 UTC 30 January (Fig. 16). Simulated column-maximum reflectivity is displayed in the colored contours with SALLJ peak strength in the purple shaded contours. At 1800 UTC, storms initiated over the southern portion of the SDC and a convective system was located on the eastern coast (Fig. 16a). By 2100 UTC, widespread unorganized storms covered an area reaching from the system to the east to the foothills of the Andes in the west (Fig. 16b). At this time, surface winds (black barbs) were northerly, but winds did not meet the SALLJ criteria at any level over much of the region. By 0000 UTC 30 January, winds strengthened to meet the SALLJ criteria in the west and main SDC regions and storms began to organize into a line just to the south (Fig. 16c). This line rapidly grew and intensified as the SALLJ also strengthened between 0300 and 0600 UTC (Figs. 16d,e).

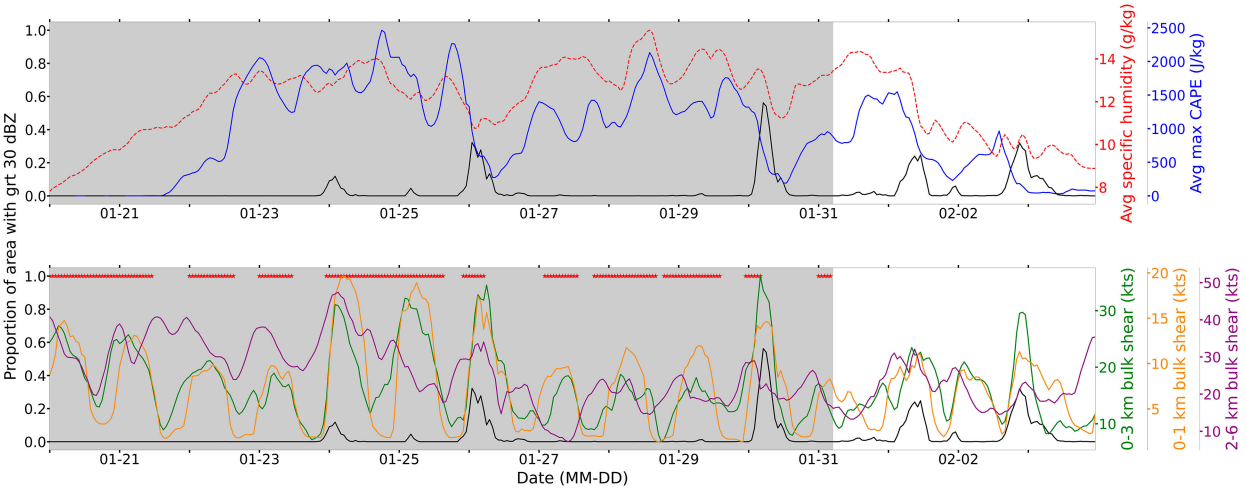

FIG. 15. As in Fig. 14, but for the west SDC region.

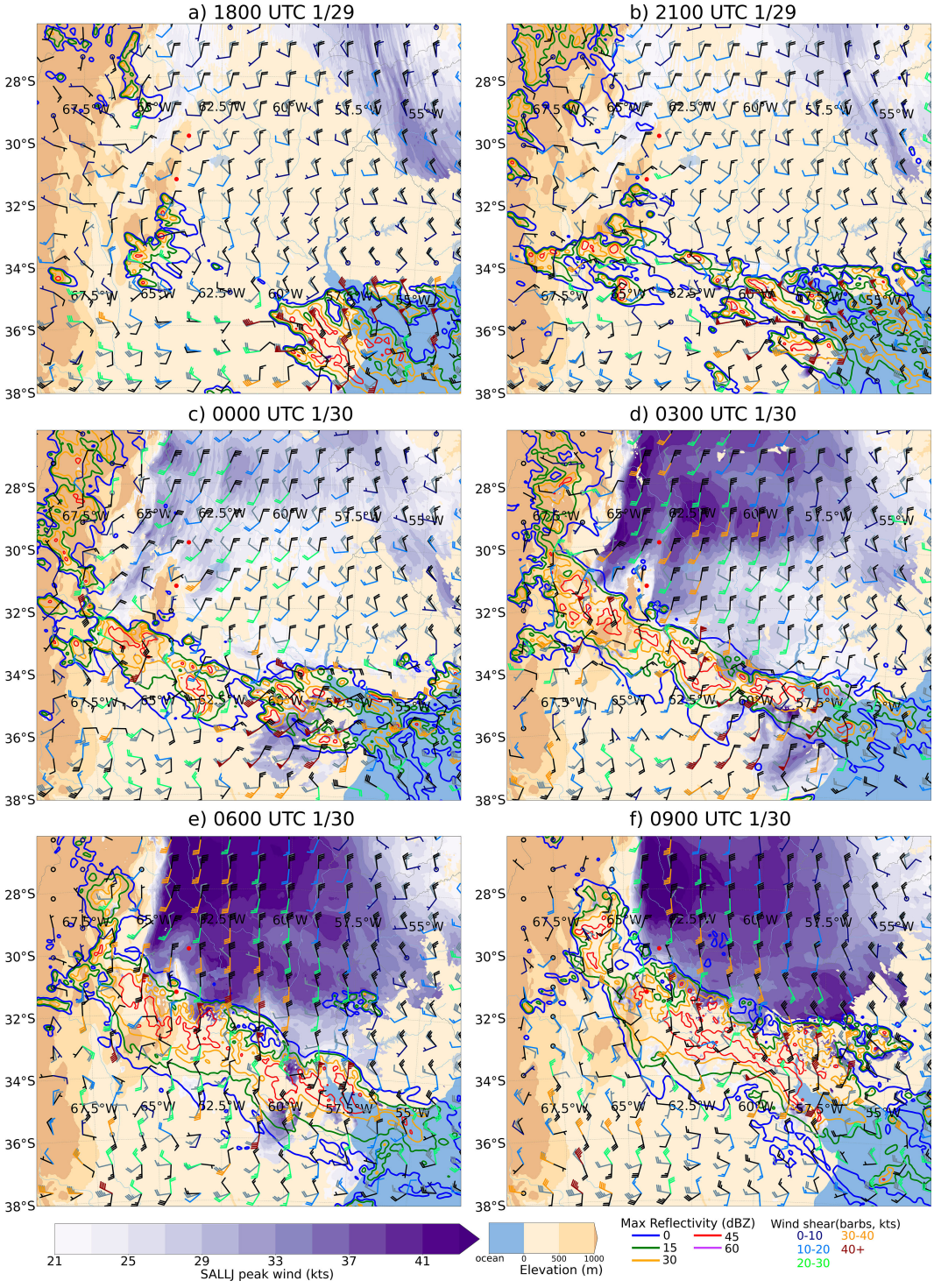

FIG. 16. Three-hourly maps of WRF simulated column-maximum reflectivity (colored contours), SALLJ peak wind speeds (purple shaded contours), surface winds (black barbs), 3-km winds (gray barbs), and 0–3-km wind shear (colored barbs). The terrain is shown in beige shading. The red dots are the locations of VMRS and COR.

The 0–3-km vertical wind shear (colored barbs in Fig. 16) increased in magnitude when the SALLJ was present during this case, particularly where the SALLJ was elevated. The shear vectors also became oriented in a southwesterly then southerly direction just ahead of the organizing convection as the SALLJ strengthened (Figs. 16d,e). In the main SDC region, both the 0–1- and 0–3-km wind shear magnitudes increased on 30 January, just prior to the increase in reflectivity coverage, while the 2–6-km

wind shear magnitude increased concurrently with the increase in reflectivity coverage (Fig. 14). In the west SDC region, 0–1- and 0–3-km wind shear also increased just prior to the growth in convective coverage, but the 2–6-km shear peaked earlier and decreased during the peak in convective coverage (Fig. 15). It is possible that this difference in timing of deep-layer shear is responsible for differences in the characteristics of the convection on either side of the SDC. The convection appears to maintain intensity longer in the main SDC region; however, determining a relationship would require further quantification of convective strength.

This case study highlights a situation where the presence of the SALLJ influences both the magnitude and direction of the wind shear at a time when convection is growing in spatial coverage near the SDC. This result suggests that variation between SALLJ periods or spatial heterogeneities within periods might mask situations or variables that are strongly influenced by the presence of the SALLJ. An examination of the conditions on a fine scale from RELAMPAGO observations is likely necessary to further understand the complex relationship between the SALLJ, the dynamic environment, and the convective characteristics during periods of upscale growth.

7. Conclusions

Convective upscale growth processes are not well represented in models but are important for the prediction of MCSs. Central Argentina is a unique place to study convective upscale growth as these processes occur over relatively small spatial and temporal scales. The SALLJ is a recurring feature during periods of upscale growth and our objective is to quantify its distribution and impact on the convective environment. Previous studies have found a maximum in SALLJ frequency near the SDC in central Argentina (e.g., Oliveira et al. 2018) with convection frequently initiating and growing rapidly upscale in this region (Mulholland et al. 2018). However, details of this maximum and the link between the SALLJ and the convective environment are not fully understood. To further this understanding, we objectively identify the SALLJ in a high-resolution 6.5-month-long WRF simulation to detail the spatial and temporal variability of the SALLJ and its impacts on the convective environment near the SDC.

Results show that the WRF simulation accurately represents the observed winds and SALLJ characteristics and provides confidence that the simulation can be used to expand on observational-based inferences of the spatial and temporal characteristics of the SALLJ. The SALLJ is most frequent during the summer to the north and west of the SDC with a secondary maximum to the east of the SDC. SALLJs are most frequently shallow (<1750 m) and display a strong overnight skew, while elevated SALLJs can occur at any time throughout the diurnal cycle. Additionally, SALLJs were found to be less frequent and more elevated near the higher terrain of the SDC. This lower frequency near the SDC is likely a result of the SALLJ often splitting around the terrain of the SDC (Froude number < 1).

Comparisons of environmental conditions during SALLJ and non-SALLJ periods show that the SALLJ has a clear impact on the thermodynamic environment, but a complex, nuanced impact on the dynamic environment. SALLJ periods often have higher amounts of low-level moisture and instability, but the impacts are not instantaneous, increasing over time when the SALLJ is present and decreasing afterward. Similar modest magnitudes of vertical wind shear were found during SALLJ and non-SALLJ periods, indicating that there are mechanisms other than the SALLJ that facilitate the production of shear in the region. When the SALLJ was located near the top of the shear layer, modest increases in 0–3-km shear were found. Slightly larger, and potentially significant, increases were present in 0–1-km shear for SALLJs that peak around 1 km. Future modeling tests are necessary to examine convective sensitivities to these changes in wind shear magnitudes.

Composite hodographs show that SALLJ periods have low-level curvature favorable for organized convection unlike non-SALLJ periods which have minimal directional shear. cloud-layer (2–6-km) shear vectors are oriented in a more north–south direction during SALLJ periods compared to non-SALLJ periods. As highlighted in previous studies, the orientation of wind shear may determine if convection grows upscale and the rate of organization (Dial et al. 2010; Mulholland et al. 2019). In cases where convection is anchored to the terrain of the SDC, the orientation of cloud-layer wind shear in a north–south direction by the SALLJ could increase the rate of upscale growth.

While large differences are not found in the magnitude of wind shear for SALLJ periods generally, results from the 29–30 January case study highlight a situation where the presence of the SALLJ influences both the magnitude and direction of the wind shear at a time when convection is growing in spatial coverage near the SDC. These results motivate additional investigations of environmental conditions during periods of upscale growth to better understand how the SALLJ contributes to favorable dynamic environments for the organization of convection.

One caveat to these results is that WRF slightly underestimated the winds close to the SDC. This underestimation may be related to differences in boundary layer mixing in the presence of complex terrain that have not yet been evaluated for this WRF simulation. Additionally, the complexity of aligning 3D spatial structures like the SALLJ with parameters that influence convection mean that there is much to learn about how many important conditions interact across space and time scales to modulate upscale growth. Given these uncertainties, observations from the RELAMPAGO-CACTI field campaign will be used in future work to identify specific environmental conditions correlated with observed convective upscale growth. Identification of these environmental conditions will allow for comparisons with other regions and further refine understanding of conditions and processes that modulate the upscale growth of deep convection.

Acknowledgments. The authors thank Stacy Brodzik for managing the data used. This research was supported by NSF Grants AGS-2146708, AGS-2146710, and AGS-1661662. Additional support was provided by the U.S. Department of Energy Office of Science Biological and Environmental Research as part of the Atmospheric System Research program. Pacific Northwest National

Laboratory is operated by Battelle for the U.S. Department of Energy under Contract DE-AC05-76RLO1830. Computing and disk storage resources for the WRF simulation were provided by the NCAR Computational and Information Systems Laboratory, the University of Utah Center for High Performance Computing, and the National Energy Research Scientific Computing Center, a DOE Office of Science User Facility supported by the Office of Science of the U.S. Department of Energy under Contract DE-AC02-05CH11231.

Data availability statement. Quality controlled RELAMPAGO soundings are available from the NCAR EOL online data archive (UCAR/NCAR–Earth Observing Laboratory 2020). Raw WRF model (version 4.1.1; Skamarock et al. 2019) output can be accessed by contacting Adam Varble (adam.varble@pnnl.gov).

REFERENCES

Campetella, C. M., and C. S. Vera, 2002: The influence of the Andes Mountains on the South American low-level flow. *Geophys. Res. Lett.*, **29**, 1826, https://doi.org/10.1029/2002GL015451.

Cancelada, M., P. Salio, D. Vila, S. W. Nesbitt, and L. Vidal, 2020: Backward adaptive brightness temperature threshold technique (BAB3T): A methodology to determine extreme convective initiation regions using satellite infrared imagery. *Remote Sens.*, **12**, 337, https://doi.org/10.3390/rs12020337.

Carroll, B. J., B. B. Demoz, and R. Delgado, 2019: An overview of low-level jet winds and corresponding mixed layer depths during PECAN. *J. Geophys. Res. Atmos.*, **124**, 9141–9160, https://doi.org/10.1029/2019JD030658.

Cohen, A. E., M. C. Coniglio, S. F. Corfidi, and S. J. Corfidi, 2007: Discrimination of mesoscale convective system environments using sounding observations. *Wea. Forecasting*, **22**, 1045–1062, https://doi.org/10.1175/WAF1040.1.

Coniglio, M. C., J. Y. Hwang, and D. J. Stensrud, 2010: Environmental factors in the upscale growth and longevity of MCSs derived from Rapid Update Cycle analyses. *Mon. Wea. Rev.*, **138**, 3514–3539, https://doi.org/10.1175/2010MWR3233.1.

Crook, N. A., and M. W. Moncrieff, 1988: The effect of large-scale convergence on the generation and maintenance of deep moist convection. *J. Atmos. Sci.*, **45**, 3606–3624, https://doi.org/10.1175/1520-0469(1988)045<3606:TEOLSC>2.0.CO;2.

Dial, G. L., J. P. Racy, and R. L. Thompson, 2010: Short-term convective mode evolution along synoptic boundaries. *Wea. Forecasting*, **25**, 1430–1446, https://doi.org/10.1175/2010WAF2222315.1.

Du, Y., Q. Zhang, Y.-L. Chen, Y. Zhao, and X. Wang, 2014: Numerical simulations of spatial distributions and diurnal variations of low-level jets in China during early summer. *J. Climate*, **27**, 5747–5767, https://doi.org/10.1175/JCLI-D-13-00571.1.

Fritsch, J. M., R. J. Kane, and C. R. Chelius, 1986: The contribution of mesoscale convective weather systems to the warm-season precipitation in the United States. *J. Climate Appl. Meteor.*, **25**, 1333–1345, https://doi.org/10.1175/1520-0450(1986)025<1333:TCOMCW>2.0.CO;2.

Garreaud, R. D., 2000: Cold air incursions over subtropical and tropical South America: Mean structure and dynamics. *Mon. Wea. Rev.*, **128**, 2544–2559, https://doi.org/10.1175/1520-0493(2000)128<2544:CAIOSS>2.0.CO;2.

Gebauer, J. G., A. Shapiro, E. Fedorovich, and P. Klein, 2018: Convection initiation caused by heterogeneous low-level jets over the Great Plains. *Mon. Wea. Rev.*, **146**, 2615–2637, https://doi.org/10.1175/MWR-D-18-0002.1.

Hersbach, H., and Coauthors, 2020: The ERA5 global reanalysis. *Quart. J. Roy. Meteor. Soc.*, **146**, 1999–2049, https://doi.org/10.1002/qj.3803.

Higgins, R. W., Y. Yao, E. S. Yarosh, J. E. Janowiak, and K. C. Mo, 1997: Influence of the Great Plains low-level jet on summertime precipitation and moisture transport over the central United States. *J. Climate*, **10**, 481–507, https://doi.org/10.1175/1520-0442(1997)010<0481:IOTGPL>2.0.CO;2.

Houze, R. A., Jr., 2004: Mesoscale convective systems. *Rev. Geophys.*, **42**, RG4042, https://doi.org/10.1029/2004RG000150.

Iacono, M. J., J. S. Delamere, E. J. Mlawer, M. W. Shepard, S. A. Clough, and W. D. Collins, 2008: Radiative forcing by long-wave greenhouse gases: Calculations with the AER radiative transfer models. *J. Geophys. Res.*, **113**, D13103, https://doi.org/10.1029/2008JD009944.

Janjić, Z. I., 1994: The step-mountain eta coordinate model: Further developments of the convection, viscous sublayer, and turbulence closure schemes. *Mon. Wea. Rev.*, **122**, 927–945, https://doi.org/10.1175/1520-0493(1994)122<0927:TSMECM>2.0.CO;2.

Ladwig, W., 2017: wrf-python (Version 1.3.4). UCAR/NCAR, accessed 23 June 2021, https://doi.org/10.5065/D6W094P1.

Marengo, J. A., W. R. Soares, C. Saulo, and M. Nicolini, 2004: Climatology of the low-level jet east of the Andes as derived from the NCEP–NCAR reanalyses: Characteristics and temporal variability. *J. Climate*, **17**, 2261–2280, https://doi.org/10.1175/1520-0442(2004)017<2261:COTLJE>2.0.CO;2.

Monin, A. S., and A. M. Obukhov, 1954: Basic laws of turbulent mixing in the surface layer of the atmosphere. *Contrib. Geophys. Inst. Acad. Sci. USSR*, **151**, 163–187.

Mulholland, J. P., S. W. Nesbitt, R. J. Trapp, K. L. Rasmussen, and P. V. Salio, 2018: Convective storm life cycle and environments near the Sierras de Córdoba, Argentina. *Mon. Wea. Rev.*, **146**, 2541–2557, https://doi.org/10.1175/MWR-D-18-0081.1.

——, ——, and ——, 2019: A case study of terrain influences on upscale convective growth of a supercell. *Mon. Wea. Rev.*, **147**, 4305–4324, https://doi.org/10.1175/MWR-D-19-0099.1.

Nakanishi, M., and H. Niino, 2006: An improved Mellor–Yamada Level-3 model: Its numerical stability and application to a regional prediction of advection fog. *Bound.-Layer Meteor.*, **119**, 397–407, https://doi.org/10.1007/s10546-005-9030-8.

——, and ——, 2009: Development of an improved turbulence closure model for the atmospheric boundary layer. *J. Meteor. Soc. Japan*, **87**, 895–912, https://doi.org/10.2151/jmsj.87.895.

Nesbitt, S. W., R. Cifelli, and S. A. Rutledge, 2006: Storm morphology and rainfall characteristics of TRMM precipitation features. *Mon. Wea. Rev.*, **134**, 2702–2721, https://doi.org/10.1175/MWR3200.1.

——, and Coauthors, 2021: A storm safari in subtropical South America: Proyecto RELAMPAGO. *Bull. Amer. Meteor. Soc.*, **102**, E1621–E1644, https://doi.org/10.1175/BAMS-D-20-0029.1.

Nicolini, M., and A. C. Saulo, 2000: ETA characterization of the 1997–1998 warm season Chaco jet cases. Preprints, *Sixth Int. Conf. on Southern Hemisphere Meteorology and Oceanography*, Santiago, Chile, Amer. Meteor. Soc., 330–331.

——, P. Salio, G. Ulke, J. Marengo, M. Douglas, J. Paegle, and E. Zipser, 2004: South American low-level jet diurnal cycle and three dimensional structure. *CLIVAR Exchanges*, No. 9, International CLIVAR Project Office, Southampton, United Kingdom, 6–8.

Nogués-Paegle, J., and K. C. Mo, 1997: Alternating wet and dry conditions over South America during summer. *Mon. Wea. Rev.*, **125**, 279–291, https://doi.org/10.1175/1520-0493(1997)125<0279:AWADCO>2.0.CO;2.

Oliveira, M. I., E. L. Nascimento, and C. Kannenberg, 2018: A new look at the identification of low-level jets in South America. *Mon. Wea. Rev.*, **146**, 2315–2334, https://doi.org/10.1175/MWR-D-17-0237.1.

Peters, J. M., E. R. Nielsen, M. D. Parker, S. M. Hitchcock, and R. S. Schumacher, 2017: The impact of low-level moisture errors on model forecasts of an MCS observed during PECAN. *Mon. Wea. Rev.*, **145**, 3599–3624, https://doi.org/10.1175/MWR-D-16-0296.1.

Piersante, J. O., K. L. Rasmussen, R. S. Schumacher, A. K. Rowe, and L. A. McMurdie, 2021: A synoptic evolution comparison of the smallest and largest MCSs in subtropical South America between spring and summer. *Mon. Wea. Rev.*, **149**, 1943–1966, https://doi.org/10.1175/MWR-D-20-0208.1.

Piscitelli, F. M., J. J. Ruiz, P. Negri, and P. Salio, 2022: A multiyear radar-based climatology of supercell thunderstorms in central-eastern Argentina. *Atmos. Res.*, **277**, 106283, https://doi.org/10.1016/j.atmosres.2022.106283.

Rasmussen, K. L., and R. A. Houze Jr., 2011: Orogenic convection in subtropical South America as seen by the TRMM satellite. *Mon. Wea. Rev.*, **139**, 2399–2420, https://doi.org/10.1175/MWR-D-10-05006.1.

——, and ——, 2016: Convective initiation near the Andes in subtropical South America. *Mon. Wea. Rev.*, **144**, 2351–2374, https://doi.org/10.1175/MWR-D-15-0058.1.

Rasmusson, E. M., and K. C. Mo, 1996: Large-scale atmospheric moisture cycling as evaluated from NMC global analysis and forecast products. *J. Climate*, **9**, 3276–3297, https://doi.org/10.1175/1520-0442(1996)009<3276:LSAMCA>2.0.CO;2.

Reinecke, P. A., and D. R. Durran, 2008: Estimating topographic blocking using a Froude number when the static stability is nonuniform. *J. Atmos. Sci.*, **65**, 1035–1048, https://doi.org/10.1175/2007JAS2100.1.

Salio, P., M. Nicolini, and A. C. Saulo, 2002: Chaco low-level jet events characterization during the austral summer season. *J. Geophys. Res.*, **107**, 4816, https://doi.org/10.1029/2001JD001315.

Sasaki, C. R. S., A. K. Rowe, L. A. McMurdie, and K. L. Rasmussen, 2022: New insights into the South American low-level jet from RELAMPAGO observations. *Mon. Wea. Rev.*, **150**, 1247–1271, https://doi.org/10.1175/MWR-D-21-0161.1.

Saulo, C., J. Ruiz, and Y. G. Skabar, 2007: Synergism between the low-level jet and organized convection at its exit region. *Mon. Wea. Rev.*, **135**, 1310–1326, https://doi.org/10.1175/MWR3317.1.

Schumacher, R. S., and K. L. Rasmussen, 2020: The formation, character and changing nature of mesoscale convective systems. *Nat. Rev. Earth Environ.*, **1**, 300–314, https://doi.org/10.1038/s43017-020-0057-7.

——, and Coauthors, 2021: Convective-storm environments in subtropical South America from high-frequency soundings during RELAMPAGO-CACTI. *Mon. Wea. Rev.*, **149**, 1439–1458, https://doi.org/10.1175/MWR-D-20-0293.1.

Seluchi, M. E., A. C. Saulo, M. Nicolini, and P. Satyamurty, 2003: The northwestern Argentinean low: A study of two typical events. *Mon. Wea. Rev.*, **131**, 2361–2378, https://doi.org/10.1175/1520-0493(2003)131<2361:TNALAS>2.0.CO;2.

Singh, I., S. W. Nesbitt, and C. A. Davis, 2022: Quasi-idealized numerical simulations of processes involved in orogenic convection initiation over the Sierras de Córdoba. *J. Atmos. Sci.*, **79**, 1127–1149, https://doi.org/10.1175/JAS-D-21-0007.1.

Skamarock, W. C., and Coauthors, 2019: A description of the Advanced Research WRF Model version 4. NCAR Tech. Note NCAR/TN-556+STR, 145 pp., https://doi.org/10.5065/1dfh-6p97.

Smith, E. N., J. G. Gebauer, P. M. Klein, E. Fedorovich, and J. A. Gibbs, 2019: The Great Plains low-level jet during PECAN: Observed and simulated characteristics. *Mon. Wea. Rev.*, **147**, 1845–1869, https://doi.org/10.1175/MWR-D-18-0293.1.

Stelten, S., and W. A. Gallus, 2017: Pristine nocturnal convective initiation: A climatology and preliminary examination of predictability. *Wea. Forecasting*, **32**, 1613–1635, https://doi.org/10.1175/WAF-D-16-0222.1.

Stensrud, D. J., 1996: Importance of low-level jets to climate: A review. *J. Climate*, **9**, 1698–1711, https://doi.org/10.1175/1520-0442(1996)009<1698:IOLLJT>2.0.CO;2.

Tao, W.-K., and J. Simpson, 1984: Cloud interactions and merging: Numerical simulations. *J. Atmos. Sci.*, **41**, 2901–2917, https://doi.org/10.1175/1520-0469(1984)041<2901:CIAMNS>2.0.CO;2.

Tewari, M., and Coauthors, 2004: Implementation and verification of the unified Noah land surface model in the WRF Model. *20th Conf. on Weather Analysis and Forecasting/16th Conf. on Numerical Weather Prediction*, Seattle, WA, Amer. Meteor. Soc., 14.2a, https://ams.confex.com/ams/84Annual/techprogram/paper_69061.htm.

Thompson, G., and T. Eidhammer, 2014: A study of aerosol impacts on clouds and precipitation development in a large winter cyclone. *J. Atmos. Sci.*, **71**, 3636–3658, https://doi.org/10.1175/JAS-D-13-0305.1.

Trapp, R. J., G. R. Marion, and S. W. Nesbitt, 2017: The regulation of tornado intensity by updraft width. *J. Atmos. Sci.*, **74**, 4199–4211, https://doi.org/10.1175/JAS-D-16-0331.1.

——, and Coauthors, 2020: Multiple-platform and multiple-Doppler radar observations of a supercell thunderstorm in South America during RELAMPAGO. *Mon. Wea. Rev.*, **148**, 3225–3241, https://doi.org/10.1175/MWR-D-20-0125.1.

Tuttle, J. D., and C. A. Davis, 2006: Corridors of warm season precipitation in the central United States. *Mon. Wea. Rev.*, **134**, 2297–2317, https://doi.org/10.1175/MWR3188.1.

UCAR/NCAR–Earth Observing Laboratory, 2020: Multi-network composite highest resolution radiosonde data, version 1.3. UCAR/NCAR–Earth Observing Laboratory, accessed 26 September 2019, https://doi.org/10.26023/GKFF-YNBJ-BV14.

Varble, A. C., and Coauthors, 2021: Utilizing a storm-generating hotspot to study convective cloud transitions: The CACTI experiment. *Bull. Amer. Meteor. Soc.*, **102**, E1597–E1620, https://doi.org/10.1175/BAMS-D-20-0030.1.

Vera, C., and Coauthors, 2006: The South American Low-Level Jet Experiment. *Bull. Amer. Meteor. Soc.*, **87**, 63–78, https://doi.org/10.1175/BAMS-87-1-63.

Walters, C. K., J. A. Winkler, S. Husseini, R. Keeling, J. Nikolic, and S. Zhong, 2014: Low-level jets in the North American Regional Reanalysis (NARR): A comparison with rawinsonde observations. *J. Appl. Meteor. Climatol.*, **53**, 2093–2113, https://doi.org/10.1175/JAMC-D-13-0364.1.

Wang, H., and R. Fu, 2004: Influence of cross-Andes flow on the South American low-level jet. *J. Climate*, **17**, 1247–1262, https://doi.org/10.1175/1520-0442(2004)017<1247:IOCFOT>2.0.CO;2.

Weisman, M. L., C. Evans, and L. Bosart, 2013: The 8 May 2009 superderecho: Analysis of a real-time explicit convective forecast. *Wea. Forecasting*, **28**, 863–892, https://doi.org/10.1175/WAF-D-12-00023.1.

Wu, Y., and S. Raman, 1998: The summertime Great Plains low level jet and the effect of its origin on moisture transport. *Bound.-Layer Meteor.*, **88**, 445–466, https://doi.org/10.1023/A:1001518302649.

Zhang, Z., A. Varble, Z. Feng, J. Hardin, and E. Zipser, 2021: Growth of mesoscale convective systems in observations and a seasonal convection-permitting simulation over Argentina. *Mon. Wea. Rev.*, **149**, 3469–3490, https://doi.org/10.1175/MWR-D-20-0411.1.